J. Fluid Mech. (1983), *vol.* 131, *pp.* 27–57
Printed in Great Britain

An update on non-stationary oblique shock-wave reflections: actual isopycnics and numerical experiments

By R. L. DESCHAMBAULT AND I. I. GLASS

Institute for Aerospace Studies, University of Toronto, 4925 Dufferin Street, Downsview, Ontario, Canada M3H 5T6

(Received 16 September 1982)

Nonstationary oblique shock-wave reflections over compressive wedges in air and argon were investigated using infinite-fringe interferometric techniques. These allowed direct, continuous and accurate observations of the isopycnics (lines of constant density) of the flow field. The initial pressures for these experiments were made as high as possible (15 to 250 torr) in order to increase the number of isopycnics and to enhance their details and distribution along the wedge surface over a shock-Mach-number range $2.0 < M_s \leqslant 8.7$. Included in the study were two cases of regular reflection (RR) and one of each single Mach reflection (SMR), complex Mach reflection (CMR) and double-Mach reflection (DMR) for air, and one RR, SMR, CMR and DMR for argon. These particular cases, which we investigated previously in N_2 and Ar using a finite-fringe technique, have been used by computational fluid dynamicists to check their finite-difference results against our experimental data. It will be shown that the isopycnic structure previously reported by us differs in detail, in most cases, from that of the present study. The major difference arises from the fact that it was only possible previously to obtain discrete points on isopycnics and along the wedge surface. Consequently, the results obtained before were not as accurate. Comparisons were made of actual wall-density distributions with numerical simulations of the density contours of the various flows obtained by a number of authors. Each numerical method displays its advantages and disadvantages in describing the details of the flow fields. The present experimental results for air are new. They are of great interest from a practical viewpoint. The experiments in argon were redone to provide better data for a gas free from real-gas effects in the range of initial conditions considered, in order to simplify the computations in the numerical simulations. Although the recent numerical simulations are better than those reported previously, additional efforts are required to improve the predictions of the shape, location and values of the isopycnics and other flow isolines in the various regions and along the wall, and to render the predictions free of computer 'noise'. It is worth noting that real-gas effects did not play any significant role in determining the various wave systems in RR, SMR, CMR and DMR; a different claim was made in our previous work. Relaxation of nitrogen in air can be seen however, at the highest shock Mach numbers ($M_s = 7.19$ and 8.70), with relaxation lengths in good agreement with accepted predictions.

1. Introduction

The study of oblique shock-wave reflection dates back to Mach (1887). It has been investigated extensively by many researchers. A comprehensive list of references and more detailed introductions and discussions can be found in Ben-Dor & Glass (1978, 1979, 1980), Ando & Glass (1981), Lee & Glass (1982) and Shirouzu & Glass (1982). To this day, not all of the features associated with this phenomenon have been explained adequately. Consequently, many laboratories in several countries have directed programmes of experimental and analytical investigations in order to clear up some of the difficulties, such as the so-called 'von Neumann' paradox (Bleakney & Taub 1949), real-gas and viscous effects and the relevance of the regions and transition lines in the shock-Mach-number and wedge-angle (M_s, θ_w)-plane.

In order to improve the experimental data for computational-fluid-dynamicists, previous cases conducted in N_2 and Ar on regular reflection (RR), single-Mach reflection (SMR), complex-Mach reflection (CMR) and double-Mach reflection (DMR) have been repeated for air and Ar using infinite-fringe interferometric techniques. Higher initial pressures were employed for these experiments, where possible up to an order of magnitude greater than in previous experiments. This gave an enhanced and detailed pattern of the isopycnics in the flow field. Many runs were repeated in order to ensure that the infinite-fringe patterns could be duplicated. No major change in the isopycnic structure could be seen from run to run given the same initial conditions. Ando (1981), in addition to his work in CO_2, repeated the experiments in N_2 using the infinite-fringe method, but at lower initial pressures. His results agree very well with those of the present work. It should be clearly understood that our previous work, using finite-fringe interferograms, was hampered by the tedious reduction of the interferometric data (Ben-Dor, Whitten & Glass 1979). Only discrete points could be obtained for the isopycnic data (sometimes too few to draw appropriate curves in some areas). This also affected the density distribution along the wedge surface. Using infinite-fringe interferograms, the isopycnics appear automatically everywhere as continuous lines. This improves the experimental density distributions in the various regions of oblique shock-wave reflections, and provides more accurate distributions along the wedge surface. Consequently, although our previous data were reasonable, the present data are much more accurate and reliable. The new results will be used by computational-fluid-dynamicists to compare their numerical simulations with actual data.

Major advances have been made in the field of numerical simulation of oblique (and spherical) shock-wave reflection. Several investigators (Book *et al.* 1981; Booen & Needham 1981; Colella & Glaz 1982; Fry *et al.* 1981; Champrey, Chaussee & Kutler 1982) have made many improvements in the simulation of isopycnics in these flow fields, showing better agreement with experimental data than had been previously obtained. This shows that impressive strides have been made in numerical simulations which can describe pseudostationary and non-stationary complex flows. The present experimental data should aid materially in developing even better and more accurate computational techniques. If agreement can be obtained between the present experimentally measured isopycnics and those predicted numerically, it would lend great confidence in the computational methods, especially for spherical blast, where no interferometric results exist. If the present isopycnic and wall-density data can be simulated with precision, then many more credible numerical results could be obtained for quantities which are usually very difficult to measure experimentally.

This would reduce the cost of conducting complex experiments in the laboratory or during blast-wave trials in special field testing grounds.

Another consideration which was not taken into account in previous experimental studies was of the effect of vibrational relaxation on shock structure. For two cases in air, $M_s = 7.19$, $p_0 = 60$ torr, $\theta_w = 20°$, and $M_s = 8.7$, $p_0 = 30.75$ torr, $\theta_w = 27°$, relaxation zones due to nitrogen vibration are clearly observed in the interferograms. Therefore non-equilibrium effects in the flow (not the reflection configuration) become important in such cases. This point will be discussed later when the above cases are treated individually.

The four basic types of pseudostationary oblique shock-wave reflection are shown in figure 1 and consist of (*a*) regular reflection – RR, (*b*) single-Mach reflection – SMR, (*c*) complex-Mach reflection – CMR, and (*d*) double-Mach reflection – DMR. The type of reflection depends, for frozen (perfect) gases, on the initial Mach number M_s and the wedge angle θ_w. If relaxation lengths are short, then the initial pressure p_0 and temperature T_0 must also be specified. Figure 1 illustrates the definitions of wedge angle θ_w, triple-point-trajectory angles χ, χ', various shock waves I, R, R', M, M', slipstreams S, S' and the flow regions (1)–(5) produced by RR, SMR, CMR and DMR reflections.

Finally, it should be noted that a great deal of money is spent every year by various agencies to obtain numerical solutions for similar problems in spherical blast. It is therefore of considerable importance to simulate numerically the wedge flows first, since the experimental data can be used to test various codes, before they are applied to the more complex spherical flows. This step would lead to greater credibility of the spherical-flow simulations.

2. Experimental procedures

The reflection experiments were conducted over steel wedges of fixed angle θ_w, in the University of Toronto Institute for Aerospace Studies (UTIAS) 10×18 cm Hypervelocity Shock Tube. A 23 cm diameter Mach–Zehnder interferometer in the infinite-fringe mode was used to record the reflection process in air and argon. The light source consisted of a giant-pulse ruby laser capable of yielding simultaneous dual-frequency interferograms at wavelengths of 6943.0 Å and 3471.5 Å. The interferograms were evaluated using a procedure outlined by Ando (1981), with previous experimental results as a guide. Further details can be found in the aforementioned references.

Since the present experiments were carried out at relatively high initial argon or air pressures compared with those of previous work, it was necessary to use combustion-driven shock waves to obtain high Mach numbers, although cold-driver gases were satisfactory for lower shock Mach numbers. The combustion runs could only be performed a limited number of times as the high-quality optical glass windows were burned slightly in such runs. This can be seen in some of the interferograms. The repeatability of the incident shock Mach number using both methods of driving shock waves into the test gas was excellent for all cases.

3. Experimental results, numerical data and discussions

The initial conditions for the different air and argon cases are listed in table 1. The aim of the study was to duplicate the initial conditions used by Ben-Dor & Glass (1978,

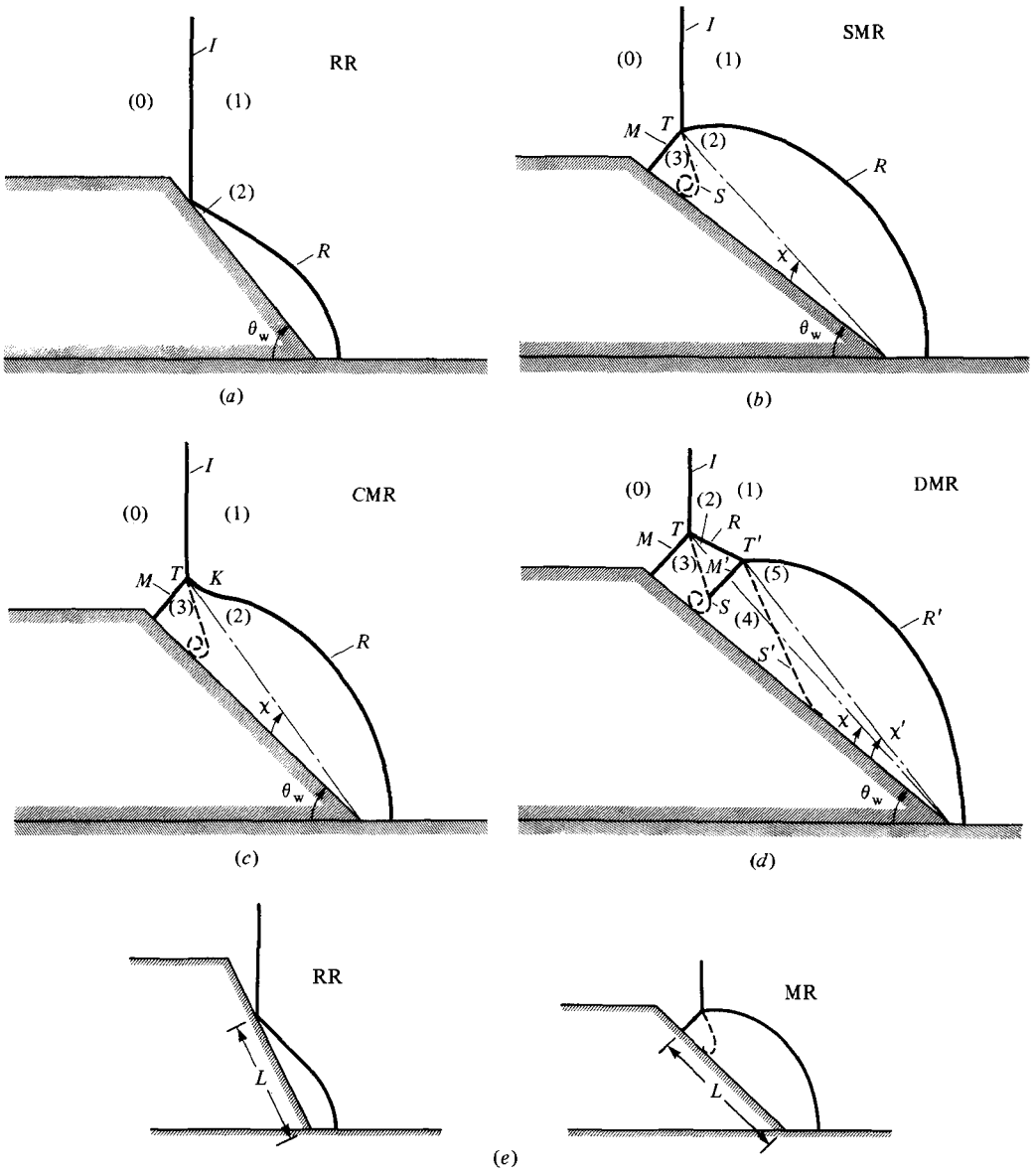

FIGURE 1. Schematic diagrams of types of pseudostationary oblique shock-wave reflection patterns: (*a*) regular reflection; (*b*) single-Mach reflection; (*c*) complex-Mach reflection; (*d*) double-Mach reflection; (*e*) definition of distance L.

1979, 1980), except for the initial pressures, which were deliberately made as high as possible to provide clearer, more numerous, and better-defined isopycnics. The test gases used were air, rather than N_2, for the diatomic case, and argon for the monatomic case. Air is of much more interest to experimenters in the field engaged in blast-wave trials. The combustion runs had Mach numbers slightly higher than in the previous work. Few calibration runs could be afforded because of damage suffered by the test section windows. The values of the flow isopycnics were normalized by the initial density in the region ahead of the incident shock wave. Consequently, the actual isopycnic shapes and values observed should be identical

Case	Gas	Type	θ_w	M_s	p_0 (torr)	T_0 (K)	ρ_0 (g/cm^3)
1	Air	RR	63.4°	2.05	250.0	298.4	3.87×10^{-4}
2	Air	RR	60.0°	4.70	46.0	298.5	7.12×10^{-5}
3	Air	SMR	27.0°	2.03	250.0	299.2	3.87×10^{-4}
4	Air	CMR	20.0°	7.19	60.0	298.5	9.29×10^{-5}
5	Air	DMR	27.0°	8.70	30.8	299.2	4.76×10^{-5}
6	Ar	RR	60.0°	2.05	150.0	297.6	3.23×10^{-4}
7	Ar	SMR	20.0°	3.20	100.0	297.7	2.15×10^{-4}
8	Ar	CMR	30.0°	5.07	30.0	298.1	6.45×10^{-5}
9	Ar	DMR	49.0°	7.10	15.0	296.3	3.29×10^{-5}

TABLE 1. Initial conditions for the various oblique shock-wave reflection cases

with those computed (accurately) regardless of the higher initial pressures, except when real-gas effects play a role.

Table 1 shows nine separate cases used for comparison purposes. Each case has been treated by several authors using a variety of numerical methods. Rather than list all the cases and describe the methods used, these details will be discussed as each case is treated individually.

3.1. *Air: cases* 1–5

Case 1: $M_s = 2.05$, $\theta_w = 63.4°$, $p_0 = 250$ torr, $T_0 = 298.4$ K, RR. The general structure of the isopycnics in air (figure 2*a*) agrees well with the results of Ando (1981) in N_2 (figure 2*b*). His experiments were performed at lower initial pressures, and consequently do not show as many isopycnics as in the present study. It can be seen that there are some discrepancies with the contours given by Ben-Dor & Glass (1978) (figure 2*c*) obtained from the finite-fringe method at discrete points. (These should have been left as points, rather than joined as lines.) In figure 2(*a*) the densities along each contour, as well as in the uniform states at the reflection point, are given. The isopycnics differ by $\Delta\rho/\rho_0 = 0.08$.

The numerical simulation by Schneyer (1975) using a 2-dimensional Eulerian code (figure 2*d*) do not represent the density contours very well. The results of Kutler & Shankar (1977) for the isopycnics (figure 2*e*), using a time-dependent 2-dimensional Eulerian code, show quite good agreement with the present study. Also, no major differences can be seen in the computed isopycnics as compared with figure 2(*b*).

The evaluation of the density along the wall surface (figure 3) agrees well with the results of Ando (1981) in N_2. His values are slightly lower, right across the wedge. This is probably due to the fact that the Mach number for the present case is higher than in Ando's case. The results of Ben-Dor & Glass (1978) do not agree well with the present data, especially in the nonuniform region behind the reflected shock. Note that $a, \ldots, g$ are specific points along the wedge surface and are replotted on the surface-density curve. (Observe also that these letters are different from those of figure 2. In figure 2(*a*) the sonic circle is at *a* whereas in figure 3 it is at *e*.) The distance *fc* is identical with *L* in figure 1(*e*), and *f* is the reflection point.

For air, a frozen (perfect) gas analysis was used to calculate the thermodynamic reference states $(0, \ldots, 2)$ around the reflection point of the RR. In all cases considered when plotting the wall-density distributions, the distance, from the point of intersection of the two shocks for RR, or from the foot of the Mach stem to the corner of the wedge, is defined as the distance *L*. This facilitates the plotting of the distance coordinate, since no scaling factors or cumbersome conversions are required (see figure 1*e*).

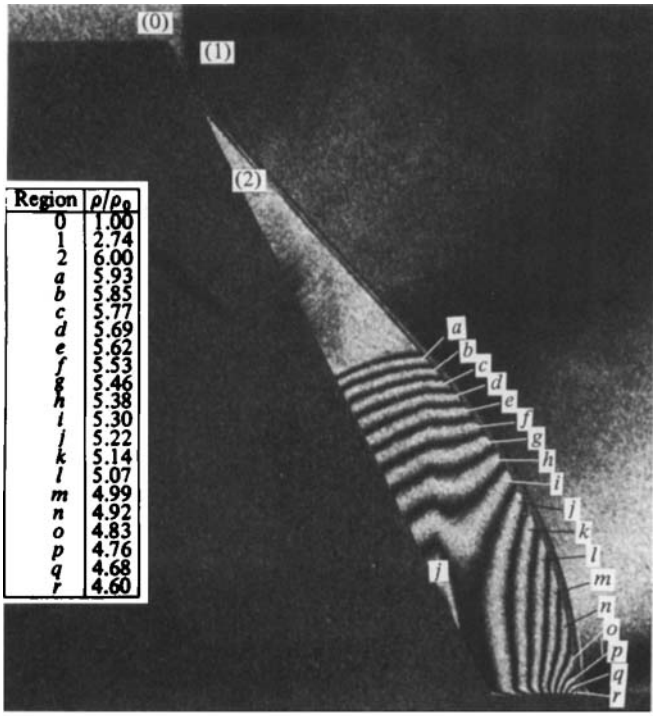

Region	ρ/ρ_0
0	1.00
1	2.74
2	6.00
a	5.93
b	5.85
c	5.77
d	5.69
e	5.62
f	5.53
g	5.46
h	5.38
i	5.30
j	5.22
k	5.14
l	5.07
m	4.99
n	4.92
o	4.83
p	4.76
q	4.68
r	4.60

(*a*)

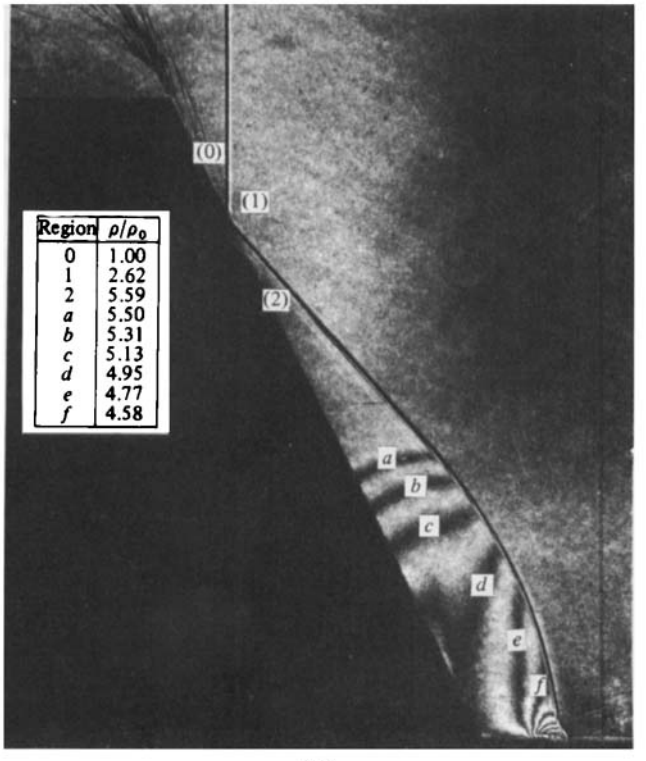

Region	ρ/ρ_0
0	1.00
1	2.62
2	5.59
a	5.50
b	5.31
c	5.13
d	4.95
e	4.77
f	4.58

(*b*)

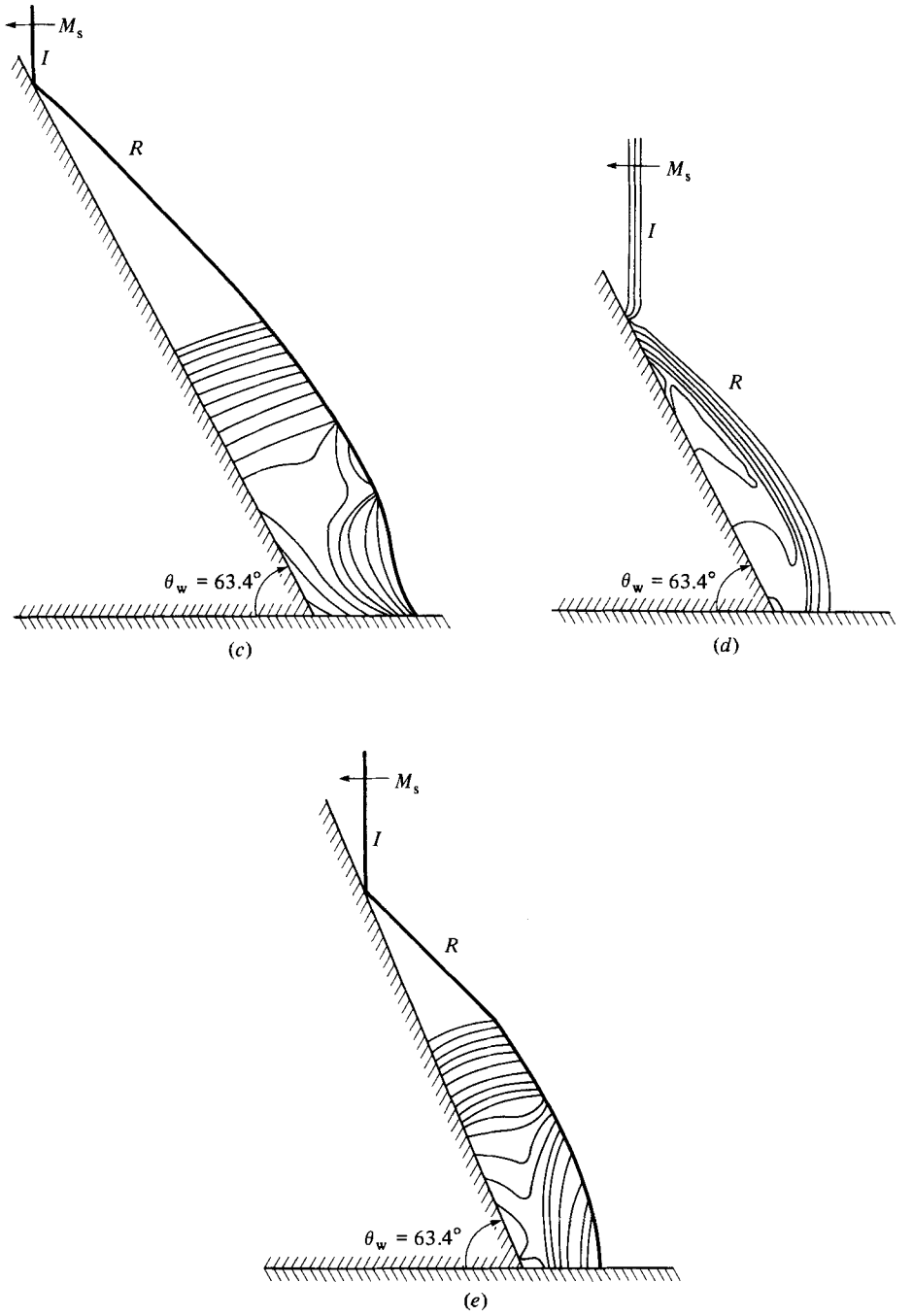

FIGURE 2. Isopycnics for regular reflection (case 1): (*a*) present experimental results, $M_s = 2.05$, $\theta_w = 63.4°$, $p_0 = 250$ torr, $\rho_0 = 3.87 \times 10^{-4}$ g/cm^3, $T_0 = 298.4$ K, $\lambda = 6943$ Å; (*b*) Ando's (1981) experimental results in nitrogen, $M_s = 1.97$, $\theta_w = 63.4°$, $p_0 = 50$ torr, $T_0 = 298.2$ K, $\rho_0 = 7.58 \times 10^{-5}$ g/cm^3, $\lambda = 3472$ Å; (*c*) isopycnics obtained from fringe-shift analysis of finite-fringe interferograms by Ben-Dor & Glass (1978), $M_s = 2.01$, $\theta_w = 63.4°$, $p_0 = 50$ torr, $T_0 = 298.6$ K; (*d*) numerical simulation of the contours of the density field by Schneyer (1975); (*e*) numerical simulation of the contours of the density field by Kutler & Shankar (1977).

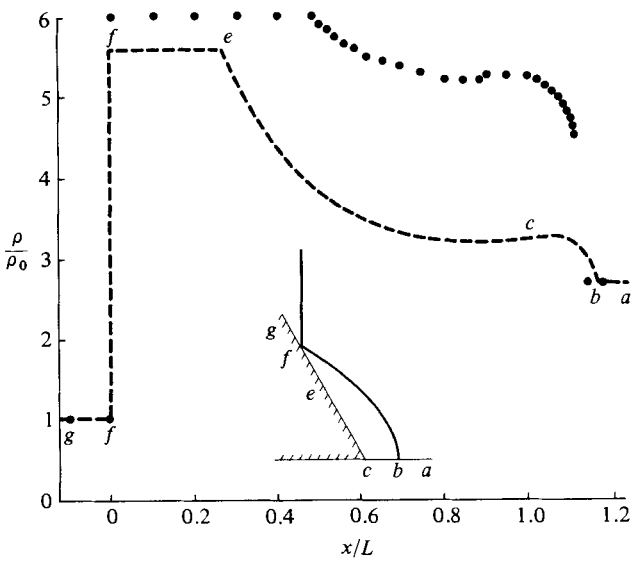

FIGURE 3. Wall-density distribution for the case of regular reflection in air (case 1): ------, Ben-Dor & Glass (1978); ●, present experimental results with an error bar given by $\Delta\rho = \pm 3.0 \times 10^{-6}$ g/cm^3. The error comes about from the fact that the fringe shift can be measured to an accuracy of 0.1 fringe.

The sudden change in density from states (0) to (2) occurs at *f*, followed by a uniform state up to the sonic circle *e* (for both evaluations but at different points) and the density then continues to drop (apart from a small rise near the corner) through the detachment distance and bow shock to the value in state (1). Here as well, there was no reason to draw this distribution as a solid line in Ben-Dor & Glass (1978) as it is composed of a finite number of data points (less than in the present work). It is shown here as a dashed line for clarity of comparison. Our data points are shown as filled-in circles.

In most cases the isopycnics of the actual interferogram at the wedge corner are extremely complicated, because of the shock-wave interaction with the boundary layer. Hence, in the wall-density plots the given density values are those above the observed boundary layer, which corresponds to the inviscid case of comparable numerical simulations.

Case 2: $M_s = 4.7, \theta_w = 60°, p_0 = 46.0$ torr, $T_0 = 298.5$ K, RR. The general structure of the density contours in air (figure 4*a*) agrees well with the results of Ando in N_2. The experimental data of Ben-Dor and Glass (figure 4*c*) show significant differences in the isopycnic shapes from those of the present study, and no uniform state (2) exists. Kutler & Shankar's time-dependent 2-dimensional Eulerian code (figure 4*d*) also predicts a uniform region behind the reflected shock which is not observed

FIGURE 4. Isopycnics for regular reflection (case 2): (*a*) present experimental results, $M_s = 4.70$, $\theta_w = 60°$, $p_0 = 45$ torr, $\rho_0 = 7.12 \times 10^{-5}$ g/cm^3, $T_0 = 298.5$ K, $\lambda = 6943$ Å; (*b*) Ando's (1981) experimental results in nitrogen, $M_s = 4.66$, $\theta_w = 63.4°$, $p_0 = 15$ torr, $T_0 = 298.3$ K, $\rho_0 = 2.26 \times 10^{-5}$ g/cm^3, $\lambda = 3472$ Å; (*c*) isopycnics obtained from fringe-shift analysis of finite-fringe interferograms by Ben-Dor & Glass (1978), $M_s = 4.68$, $\theta_w = 60°$, $p_0 = 15.31$ torr, $T_0 = 298.1$ K; (*d*) numerical prediction of the isopycnics for regular reflection by Kutler & Shankar (1977).

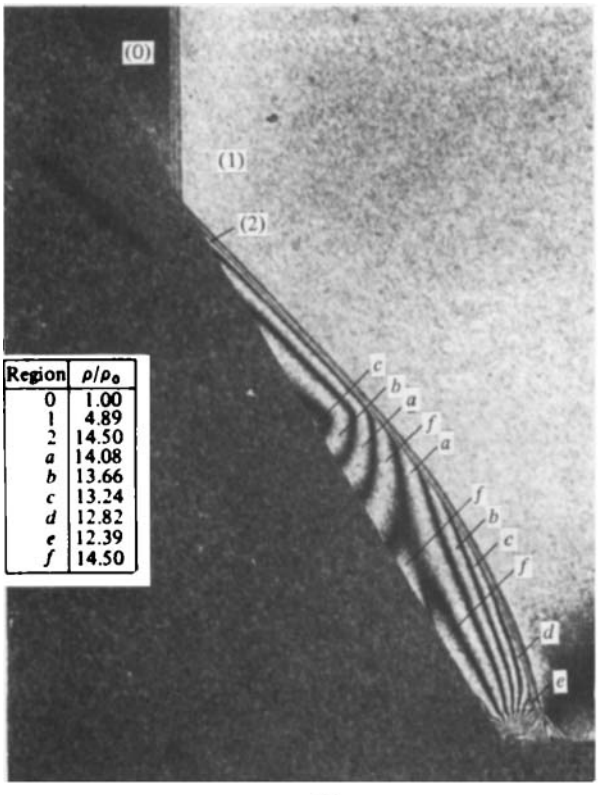

Region	ρ/ρ_0
0	1.00
1	4.89
2	14.50
a	14.08
b	13.66
c	13.24
d	12.82
e	12.39
f	14.50

(*a*)

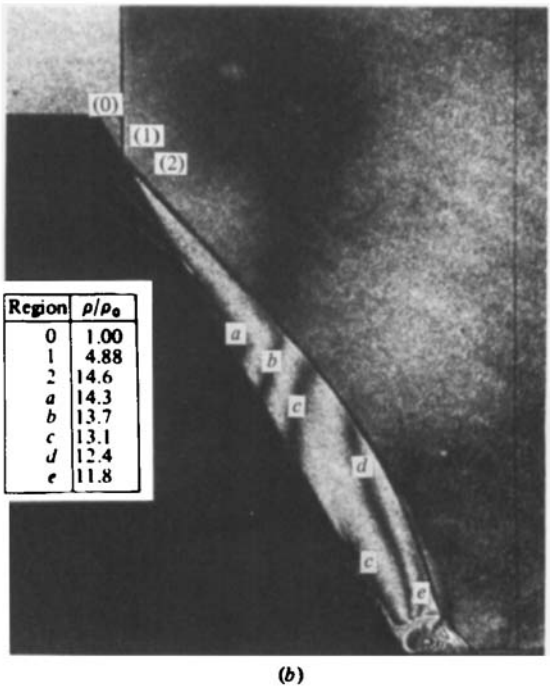

Region	ρ/ρ_0
0	1.00
1	4.88
2	14.6
a	14.3
b	13.7
c	13.1
d	12.4
e	11.8

(*b*)

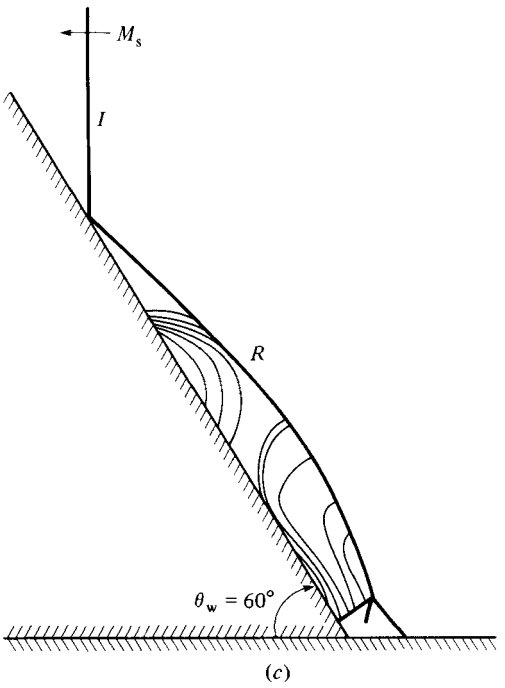

(*c*)

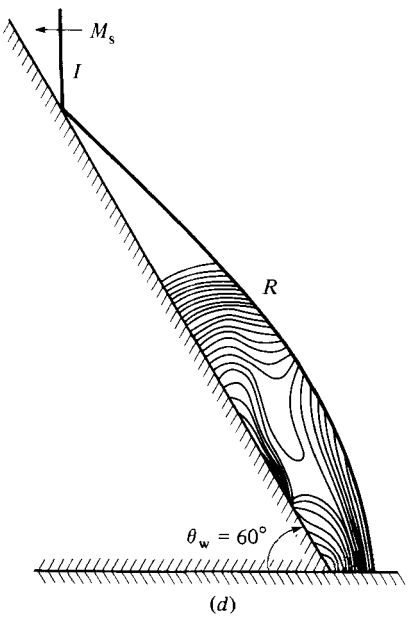

(*d*)

FIGURE 4. For caption see facing page.

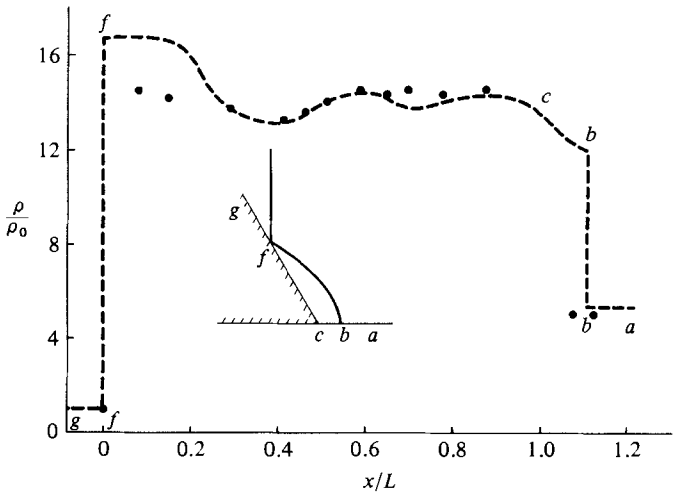

FIGURE 5. Wall-density distribution for the case of regular reflection in air (case 2): ———, by Ben-Dor & Glass (1978); ●, present experimental results, $\Delta\rho = \pm 3.0 \times 10^{-6}$ g/cm^3.

experimentally. Ben-Dor & Glass (1978) erroneously suggest that a real-gas analysis would be appropriate. The wall-density distribution (figure 5) obtained using a frozen (perfect) gas analysis in the present study is correct in view of the long vibrational relaxation times for N_2.

Ben-Dor & Glass differentiated correctly between cases 2 and 1, as far as the diffraction processes are concerned. The flow behind the incident shock wave for case 1 is subsonic, whereas in case 2 the flow behind the incident wave is supersonic. The reflected bow wave R is able to propagate upstream in case 1 but is in a fixed position for case 2. The shock-wave/boundary-layer interaction is also much stronger for case 2 than in case 1, as seen in the interferograms.

Case 3: $M_s = 2.03$, $\theta_w = 27.0°$, $p_0 = 250$ torr, $T_0 = 299.2$ K, SMR. The general shapes of the isopycnics (figure 6*a*) agree very well with the results of Ando in N_2 (figure 6*b*). Again, differences are seen between the contours of Ben-Dor & Glass (1978) (figure 6*c*) and the present study, especially in the region behind the triple point along the reflected shock. No isopycnic convergence is seen in the air result in this region; hence no weak compression wave can be formed to generate a kink K. Ben-Dor & Glass anticipated the CMR case 4, without the necessary evidence. Neither has state (3) any isopycnic structure, unlike figure 6(*c*). The growth of the slipstream region with distance is well illustrated. The numerical results by Schneyer (1975) (figure 6*d*), using a Lagrangian code, give a poor representation of the density field. The wall-density distribution reported by Ben-Dor & Glass is in reasonably good agreement with the present work (figure 7), except in the bow-shock region.

Case 4: $M_s = 7.19$, $\theta_w = 20.0°$, $p_0 = 60$ torr, $T_0 = 298.5$ K, CMR. The general structure of the isopycnics in air (figure 8*a*) agrees with the results of Ando (1981) in N_2 (figure 8*b*). The results of Ben-Dor & Glass (1979) (figure 8*c*) disagree with the present study, especially in the region near the triple point and at the kink in the reflected shock. Here the density contours converge, but not in the manner they described. Again, it was an anticipated rather than an actual result. The contours also converge near the rolled-up slipstream, indicating an increase in stagnation pressure causing the roll-up. It is worth comparing figure 8(*b*) in N_2 with figure 8(*a*) in air at higher density. Fewer isopycnics exist in N_2, as expected, owing to the low

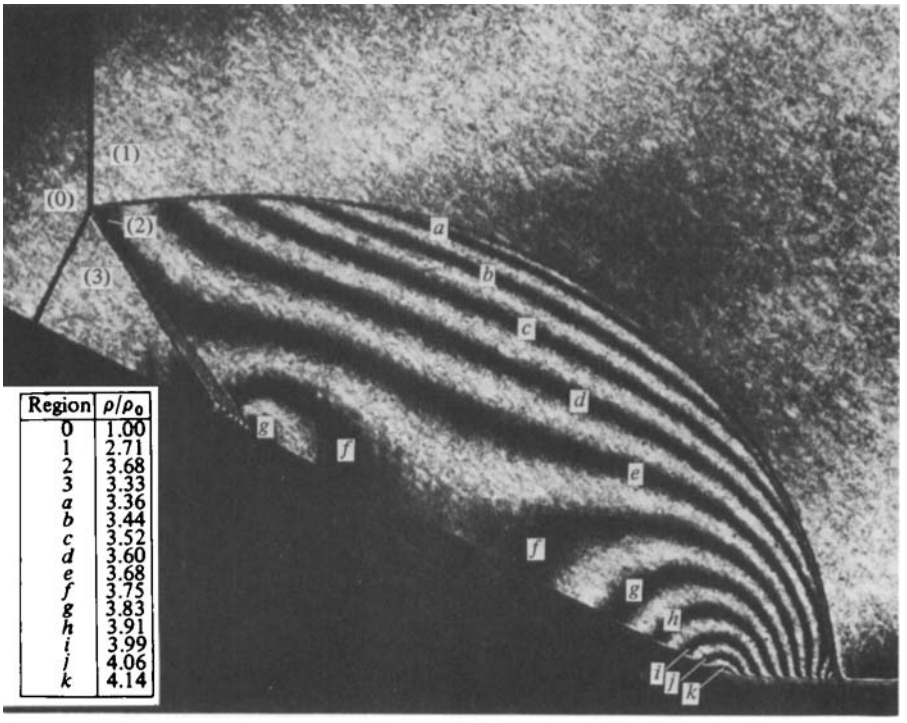

(*a*)

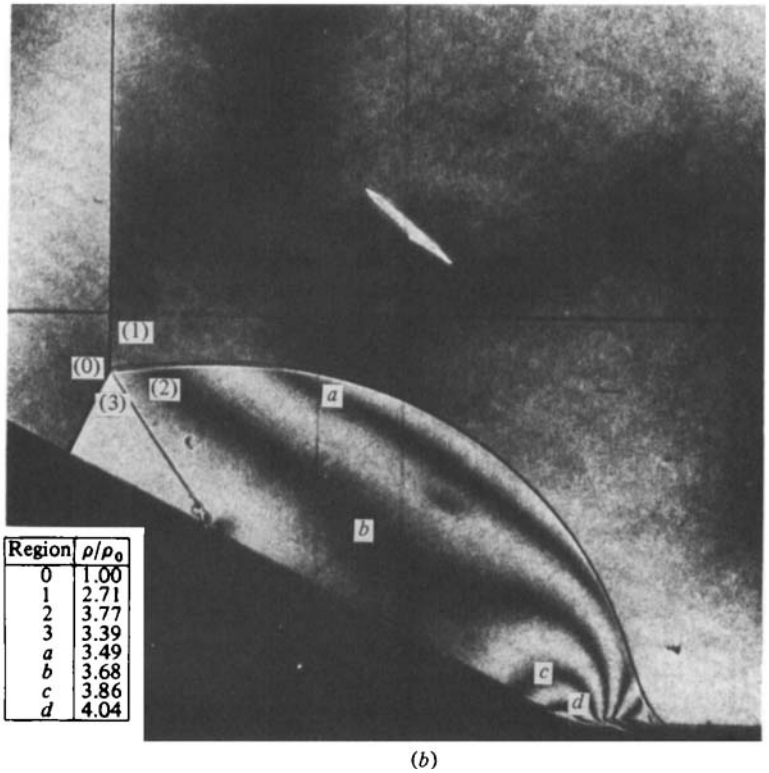

(*b*)

FIGURE 6. For caption see p. 38.

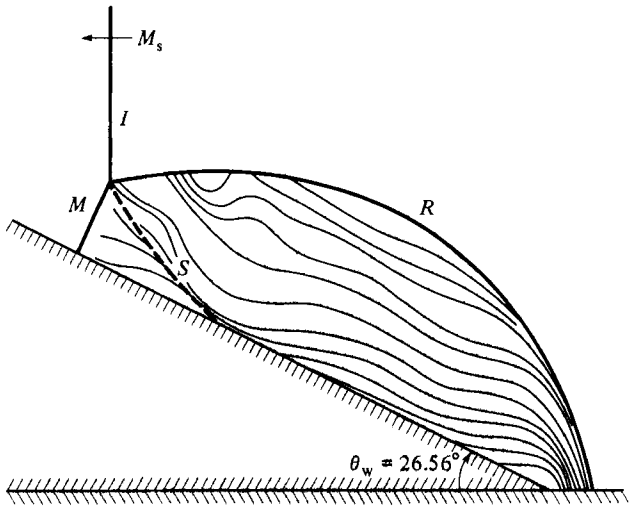

(c)

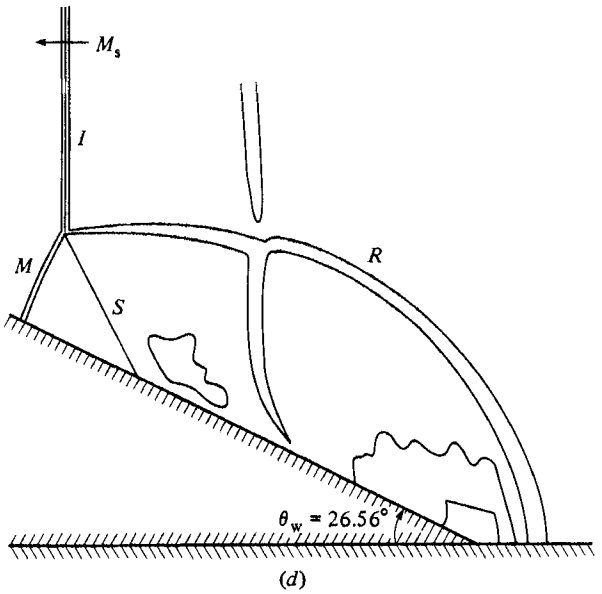

(d)

FIGURE 6. Isopycnics for single-Mach reflection (case 3): (*a*) present experimental results, $M_s = 2.03$, $\theta_w = 27°$, $p_0 = 250$ torr, $\rho_0 = 3.87 \times 10^{-4}$ g/cm^3, $T_0 = 299.2$ K, $\lambda = 6943$ Å; (*b*) Ando's (1981) experimental results in nitrogen, $M_s = 2.03$, $\theta_w = 27°$, $p_0 = 50$ torr, $\rho_0 = 7.58 \times 10^{-5}$ g/cm^3, $T_0 = 296.8$ K, $\lambda = 3472$ Å; (*c*) isopycnics obtained from fringe-shift analysis of finite-fringe interferograms by Ben-Dor & Glass (1978), $M_s = 2.01$, $\theta_w = 26.56°$, $p_0 = 50$ torr, $T_0 = 296.6$ K; (*d*) numerical simulation of the contours of the density field by Schneyer (1975), $M_s = 2$, $\theta_w = 25.56°$.

initial pressure. Consequently, the relaxation process (in the form of two fringes), mainly due to N_2 vibration, is seen behind the shock wave in state (1) in air but not in N_2. The contribution from O_2 vibration is small with a concentration of 20 %.

Using a flux-corrected-transport (FCT) algorithm in their numerical simulation, Book *et al.* (1980) show a reasonable isopycnic structure, but numerical 'noise' appears to be prevalent throughout (figure 8*d*). Booen & Nedham (1981) (figure 8*e*), using a 2-dimensional Eulerian hydrodynamic code, show more stable isopycnics and

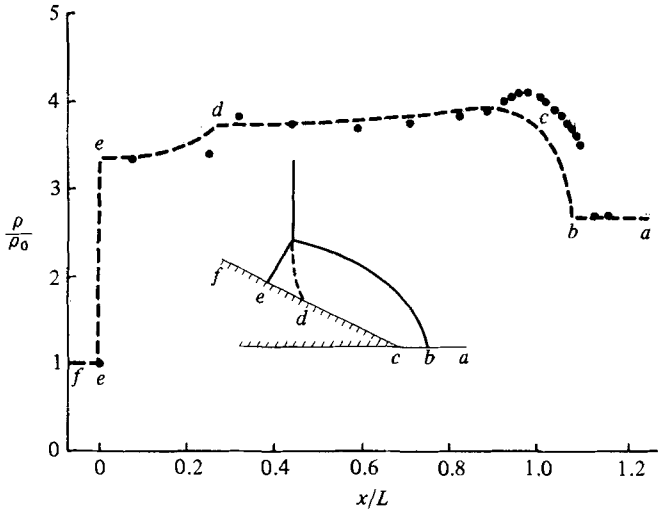

FIGURE 7. Wall-density distribution for the case of single-Mach reflection in air (case 3): ———, by Ben-Dor & Glass (1978); ●, present experimental results, $\Delta\rho = \pm 3.0 \times 10^{-6}$ g/cm^3.

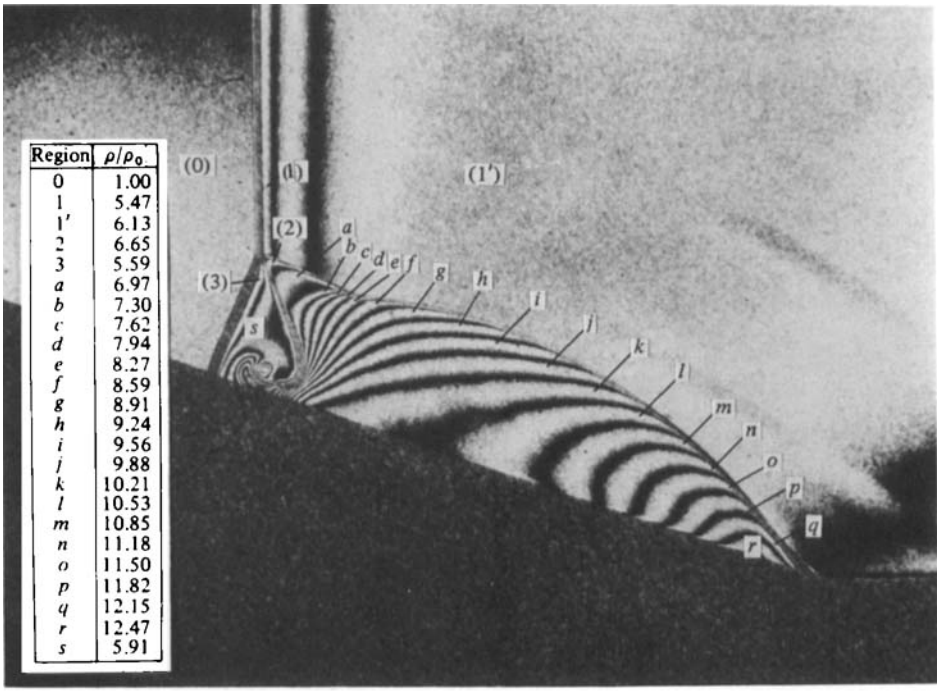

Region	ρ/ρ_0
0	1.00
1	5.47
1'	6.13
2	6.65
3	5.59
a	6.97
b	7.30
c	7.62
d	7.94
e	8.27
f	8.59
g	8.91
h	9.24
i	9.56
j	9.88
k	10.21
l	10.53
m	10.85
n	11.18
o	11.50
p	11.82
q	12.15
r	12.47
s	5.91

(*a*)

FIGURE 8. For caption see p. 41.

a well-defined structure associated with the slipstream. The wall-density distribution (figure 9) shows general agreement between the experimental and computed data. The present results for the wedge-corner region (*ba*) do show a slight drop in density before the bow shock. This was one of the high-Mach-number runs, and was accomplished by using a combustion driver.

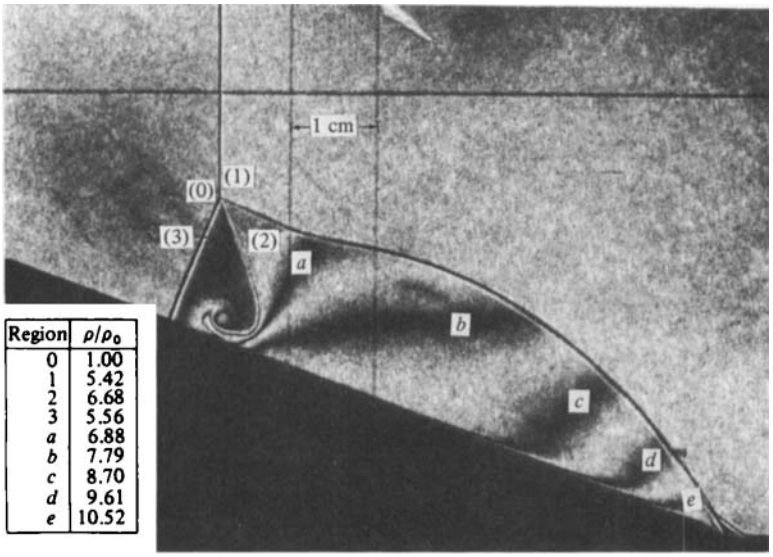

Region	ρ/ρ_0
0	1.00
1	5.42
2	6.68
3	5.56
a	6.88
b	7.79
c	8.70
d	9.61
e	10.52

(*b*)

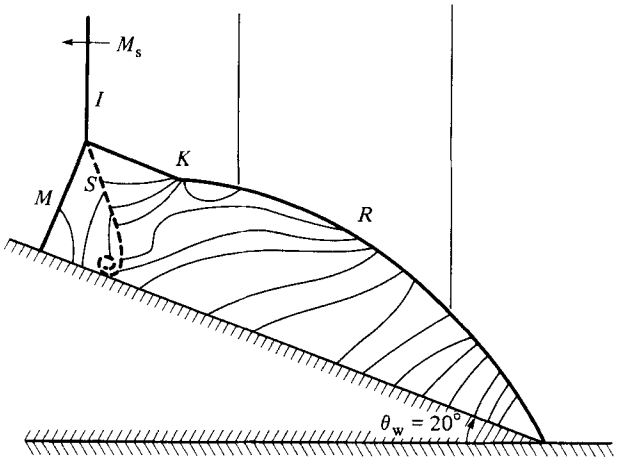

(*c*)

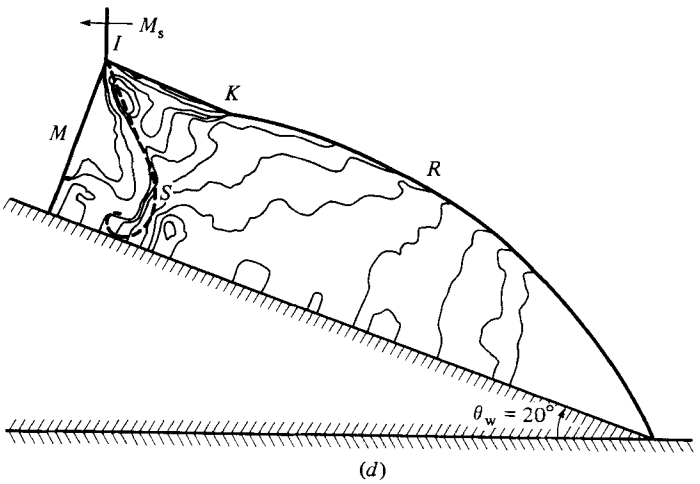

(*d*)

FIGURE 8. For caption see facing page.

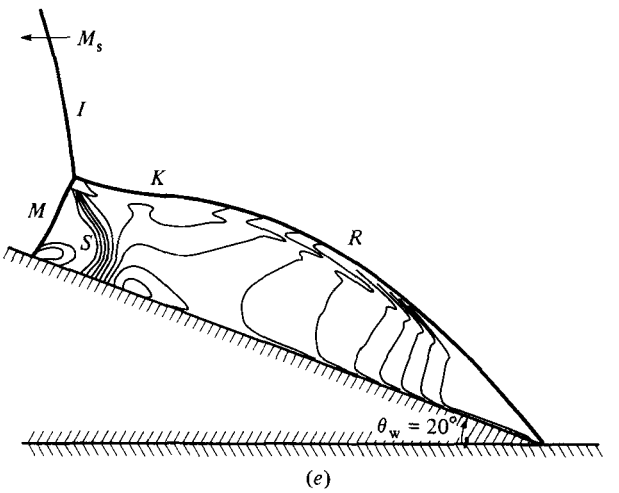

FIGURE 8. Isopycnics for complex-Mach reflection (case 4): (*a*) present experimental results, $M_s = 7.19$, $\theta_w = 20°$, $p_0 = 60$ torr, $\rho_0 = 9.29 \times 10^{-5}$ g/cm^3, $T_0 = 298.5$ K, $\lambda = 6943$ Å; (*b*) Ando's (1981) experimental results in nitrogen, $M_s = 6.8$, $\theta_w = 20°$, $p_0 = 10$ torr, $\rho_0 = 1.54 \times 10^{-5}$ g/cm^3, $T_0 = 296.2$ K, $\lambda = 3472$ Å; (*c*) isopycnics obtained from fringe-shift analysis by Ben-Dor & Glass (1979), $M_s = 6.9$, $\theta_w = 20°$, $p_0 = 10.12$ torr, $T_0 = 295.8$ K; (*d*) numerical simulation of the density contours by Book *et al.* (1980), $M_s = 6.9$, $\theta_w = 20°$; (*e*) numerical simulation of the density contours by Booen & Needham (1981), $M_s = 6.9$, $\theta_w = 20°$.

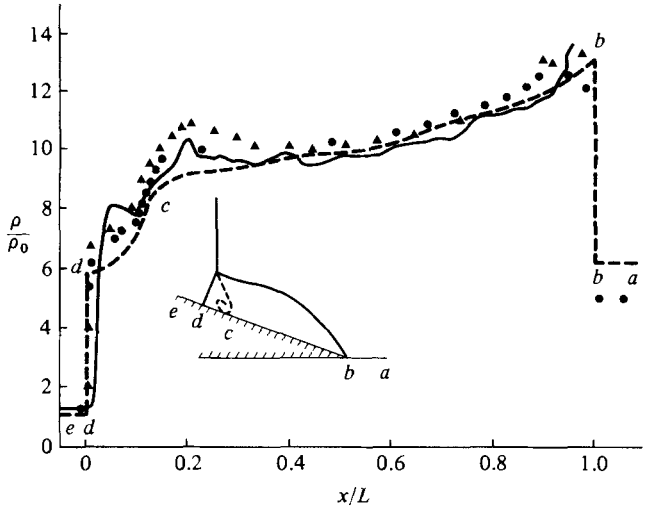

FIGURE 9. Wall density distribution for the case of complex-Mach reflection in air (case 4); – – – –, by Ben-Dor & Glass (1979); ———, by Book *et al.* (1980); ▲, by Booen & Needham (1981); ●, present experimental results, $\Delta\rho = \pm 3.0 \times 10^{-6}$ g/cm^3.

Case 5: $M_s = 8.70$, $\theta_w = 27.0°$, $p_0 = 30.8$ torr, $T_0 = 299.2$ K, DMR. Because of the limitations of cold-gas drivers in producing stronger shocks, the initial pressures used by Ando (1981) and Ben-Dor & Glass (1979) were quite low. The results for air (figure 10(*a*), done at a much higher initial pressure, show significant detail in the isopycnic structure. Ando's result is shown in figure 10(*b*). The nitrogen relaxation process in state (1) is well illustrated in figure 10(*a*). The second Mach stem and the rolled-up slipstream are particularly clear in figure 10(*b*), despite the lower initial pressure. It

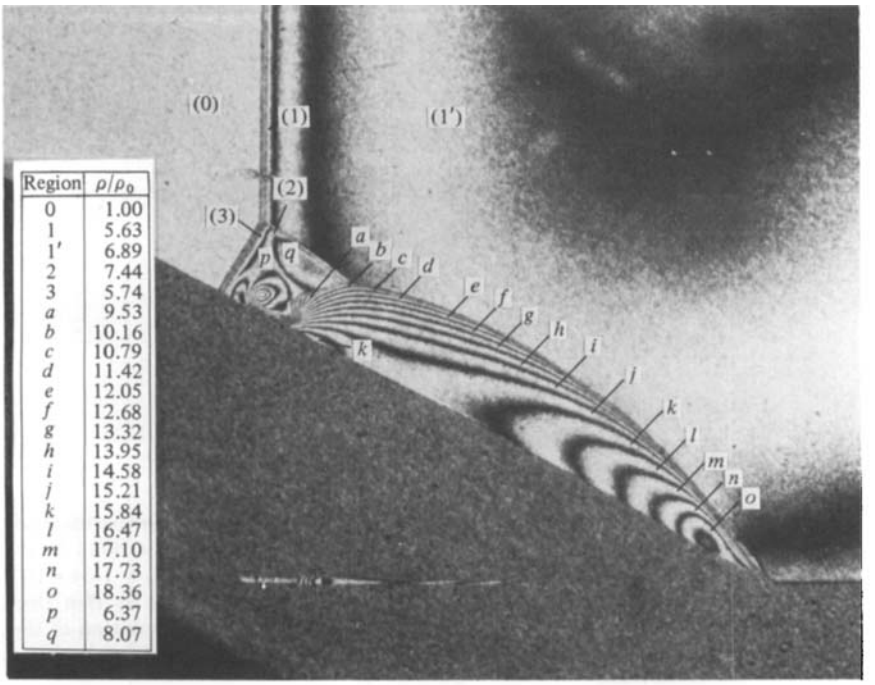

Region	ρ/ρ_0
0	1.00
1	5.63
1′	6.89
2	7.44
3	5.74
a	9.53
b	10.16
c	10.79
d	11.42
e	12.05
f	12.68
g	13.32
h	13.95
i	14.58
j	15.21
k	15.84
l	16.47
m	17.10
n	17.73
o	18.36
p	6.37
q	8.07

(*a*)

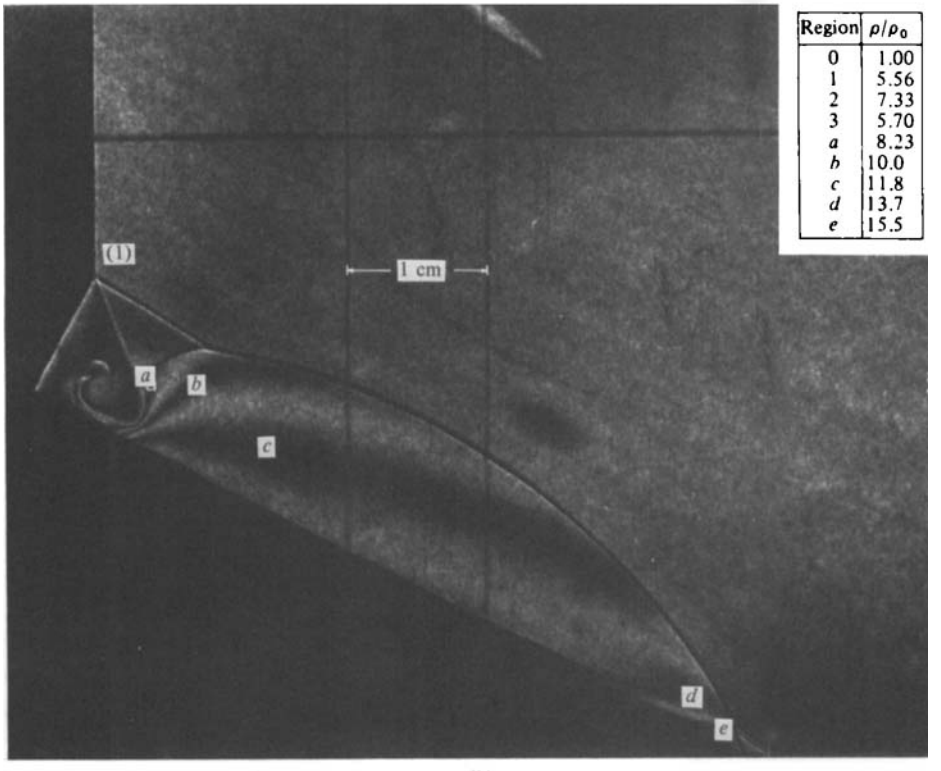

Region	ρ/ρ_0
0	1.00
1	5.56
2	7.33
3	5.70
a	8.23
b	10.0
c	11.8
d	13.7
e	15.5

(*b*)

FIGURE 10. For caption see p. 44.

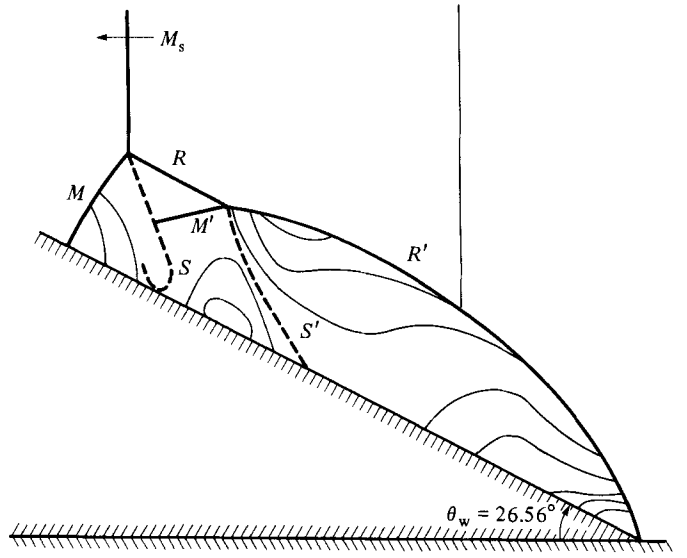

(*c*)

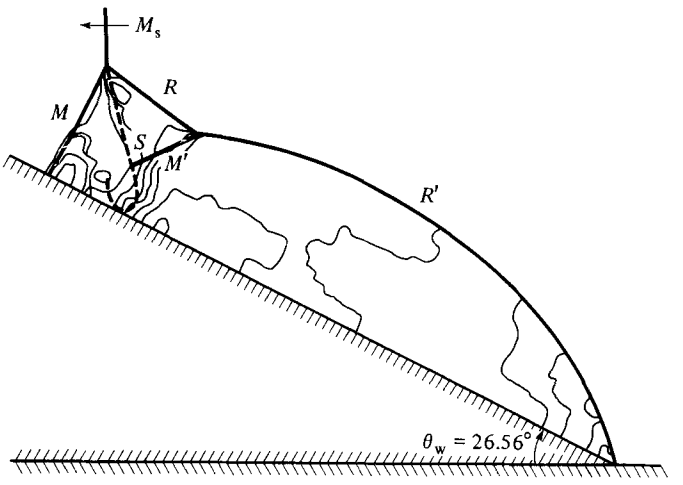

(*d*)

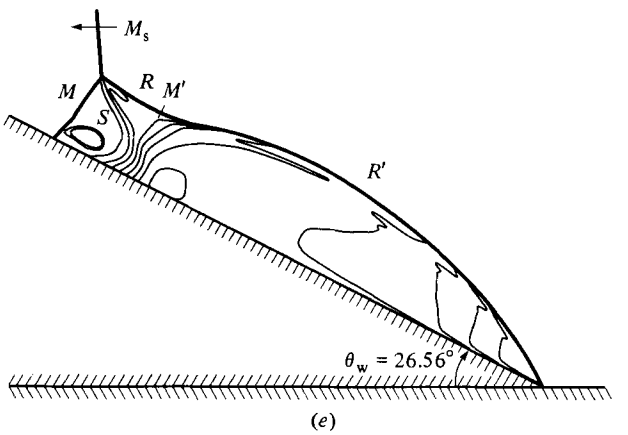

(*e*)

FIGURE 10. For caption see p. 44.

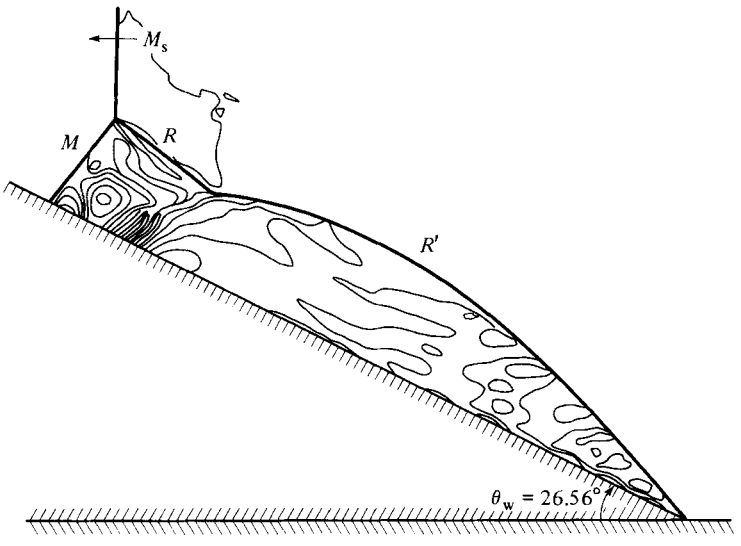

(f)

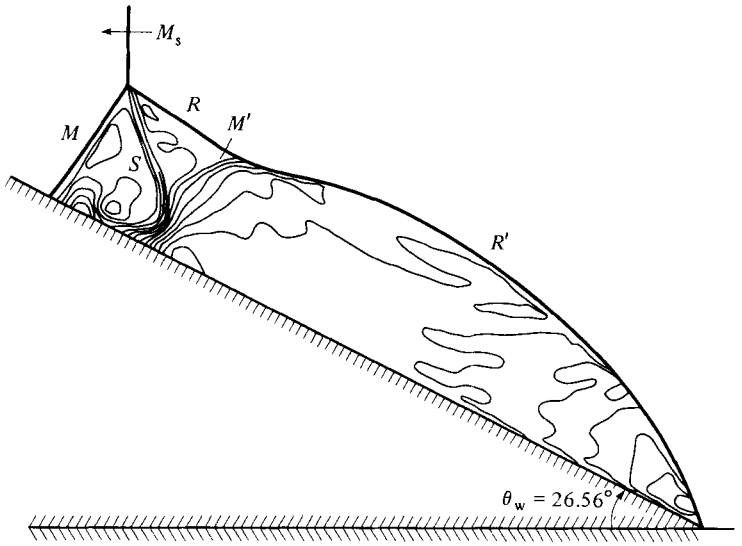

(g)

FIGURE 10. Isopycnics for double-Mach reflection (case 5); (*a*) present experimental results, $M_s = 8.70$, $\theta_w = 27°$, $p_0 = 30.80$ torr, $\rho_0 = 4.76 \times 10^{-5}$ g/cm^3, $T_0 = 299.2$ K, $\lambda = 6943$ Å; (*b*) Ando's (1981) experimental results in nitrogen, $M_s = 7.9$, $\theta_w = 27°$, $p_0 = 5$ torr, $\rho_0 = 7.69 \times 10^{-6}$ g/cm^3, $T_0 = 295.2$ *K*, $\lambda = 3472$ A; (*c*) isopycnics obtained from fringe-shift analysis by Ben-Dor & Glass (1979), $M_s = 8.06$, $\theta_w = 26.56°$, $p_0 = 5.11$ torr, $T_0 = 298.2$ K; (*d*) numerical simulation of the density contours by Book *et al.* (1981), $M_s = 8.06$, $\theta_w = 26.56°$; (*e*) numerical simulation of the density contours by Booen & Needham (1981), $M_s = 8.06$, $\theta_w = 26.56°$; (*f*) numerical simulation of density contours using real air equation of state by Colella & Glaz (1982), $M_s = 8.06$, $\theta_w = 26.56°$, (*g*) numerical simulation of density contours using constant $\gamma = 1.35$ by Colella & Glaz (1982), $M_s = 8.06$, $\theta_w = 26.56°$.

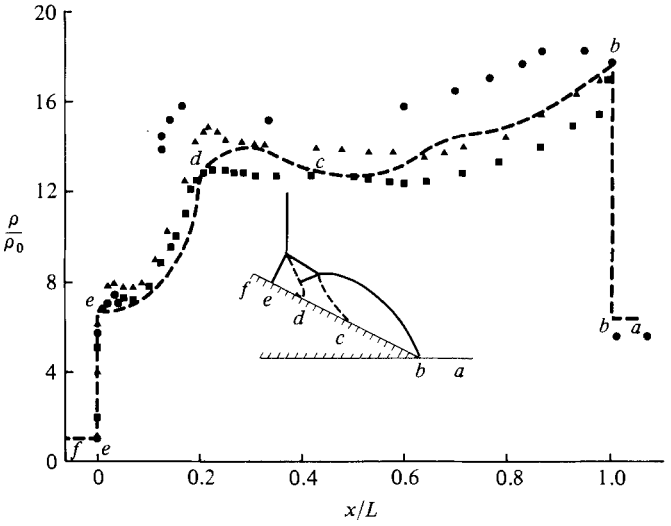

FIGURE 11. Wall-density distribution for the case of double-Mach reflection in air (case 5); ———, by Ben-Dor & Glass (1979); ▲, $\gamma = 1.30$, ■, $\gamma = 1.32$ by Booen & Needham (1981); ●, present experimental results, $\Delta\rho = \pm 3.0 \times 10^{-6}$ g/cm^3.

is worth noting that the slipstream hardly shows in figure 10(*a*) and yet is prominent in figure 10(*b*), indicating the usefulness of conducting runs at different initial conditions. Again, in comparison with Ben-Dor & Glass (figure 10*c*), differences can be seen, especially in the region around the second triple point, where no convergence of isopycnics takes place in the interferogram. The analysis of Book *et al.* shows a reasonable description of the structure in the vicinity of the Mach stems (figure 10*d*), but a poor isopycnic distribution elsewhere. Numerical noise is still apparent. Booen & Needham's model (figure 10*e*) gives a good isopycnic structure in the vicinity of the Mach stems. Again, the slipstream is well modelled. However, elsewhere the isopycnics are not well represented. The isopycnics calculated by Colella & Glaz (1982) using both frozen (perfect) and equilibrium gas models (figure 10*f*, *g*) show realistic density contours, especially in the area around the Mach stems and first slipstream. However, numerical noise is prevalent elsewhere throughout the structure. It is interesting to note that the results of real air simulate the interferogram better than the assumption $\gamma = 1.35$. The present data show a slightly higher wall-density distribution (figure 11) than that shown by Booen & Needham. This can be explained by the fact that the case of air was conducted at a higher Mach number than the other experiments. The wall-density distribution shown by Ben-Dor & Glass (1979) shows minor differences with the present work in the region close to the wedge corner. This second run attained the highest Mach-number value in the present set of experiments. A combustion driver was required for this purpose.

3.2. *Argon: cases* 6–9

All shocks were produced using a cold driver gas. As for the air cases, infinite-fringe interferometry was used to study the isopycnics of the various reflections. Where possible, higher initial pressures were again used to enhance the number of isopycnics. However, argon, with its low index of refraction, does not show as much detail in the density contours as does air. The advantage in using argon rather than air is that real-gas effects are absent; hence the task of analysis and simulation of these flows is greatly simplified. In all cases considered, a frozen (perfect) gas analysis was used

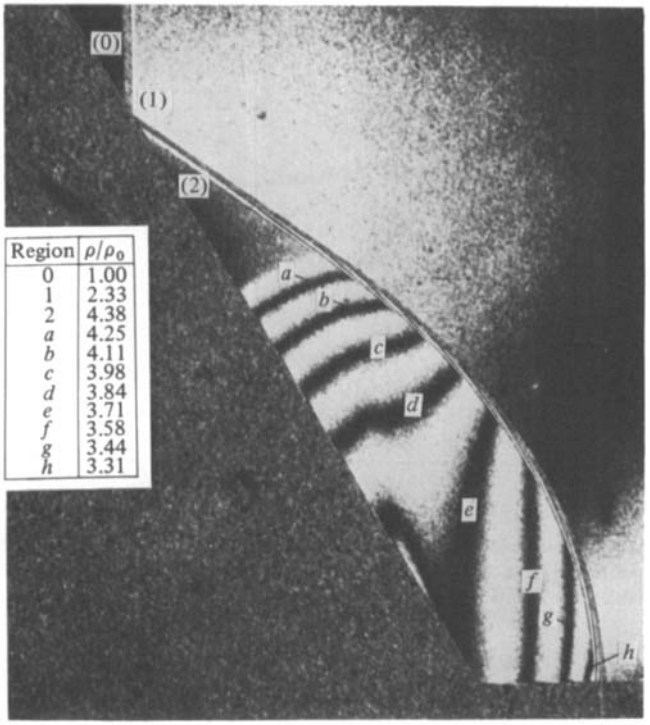

Region	ρ/ρ_0
0	1.00
1	2.33
2	4.38
a	4.25
b	4.11
c	3.98
d	3.84
e	3.71
f	3.58
g	3.44
h	3.31

(*a*)

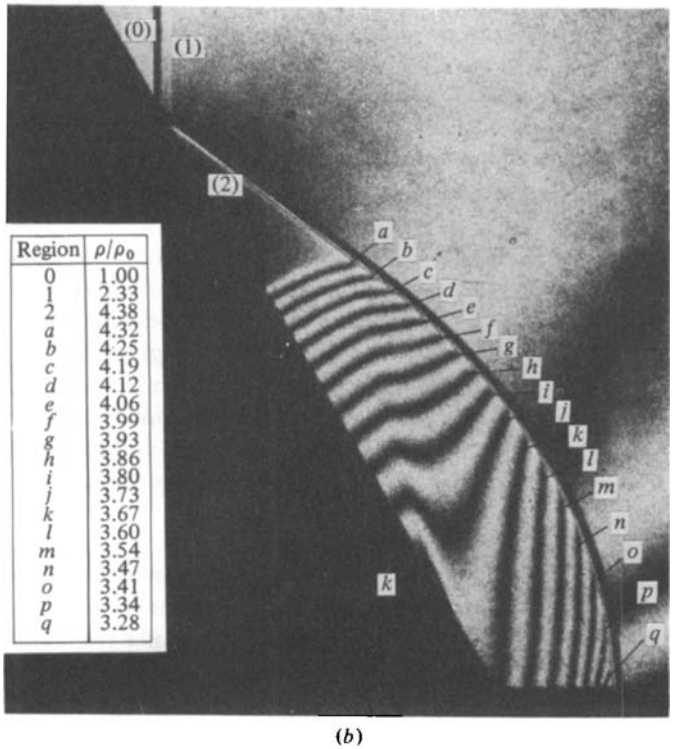

Region	ρ/ρ_0
0	1.00
1	2.33
2	4.38
a	4.32
b	4.25
c	4.19
d	4.12
e	4.06
f	3.99
g	3.93
h	3.86
i	3.80
j	3.73
k	3.67
l	3.60
m	3.54
n	3.47
o	3.41
p	3.34
q	3.28

(*b*)

FIGURE 12. For caption see facing page.

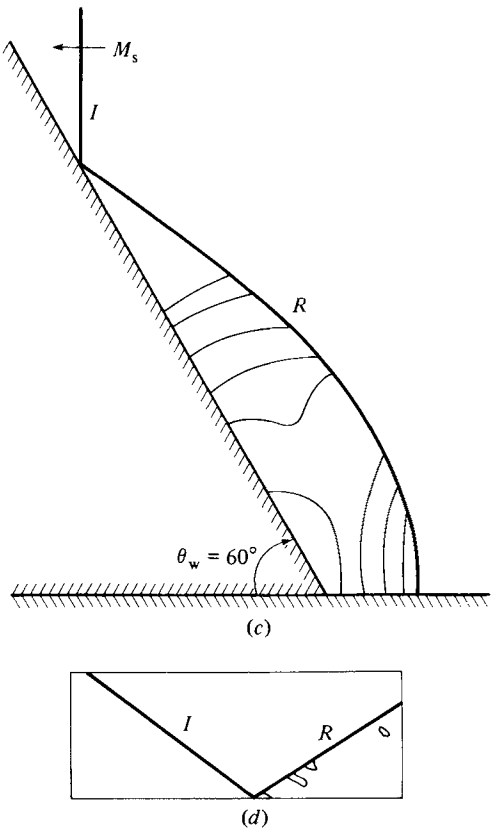

FIGURE 12. Isopycnics for regular reflection in argon (case 6); (*a*) present experimental results, $M_s = 2.05$, $\theta_w = 60°$, $p_0 = 150$ torr, $\rho_0 = 3.23 \times 10^{-4}$ g/cm^3, $T_0 = 297.6$ K, $\lambda = 6943$ Å; (*b*) present experimental results, initial conditions as above, $\lambda = 3472$ Å; (*c*) isopycnics obtained from fringe-shift analysis, by Ben-Dor & Glass (1980), $M_s = 2.03$, $\theta_w = 60°$; (*d*) numerical simulation of the density field, by Fry *et al.* (1981).

since argon has no rotational or vibrational modes to be considered and the onset of electronic excitation and ionization does not occur for $M_s \leqslant 7$, used in the present work.

Case 6: $M_s = 2.05$, $\theta_w = 60°$, $p_0 = 150$ torr, $T_0 = 297.6$ K, RR. The shapes of the isopycnics in the present study, which are given for $\lambda = 6943.0$ Å in figure 12(*a*) and in even more detail in figure 12(*b*) for $\lambda = 3471.5$ Å, show good agreement with the density contours reported by Ben-Dor & Glass (1980) (figure 12*c*), as well as in the density values themselves. The FCT numerical simulation of Fry *et al.* (1981) (figure 12*d*) shows only the uniform region behind the reflected shock wave. Therefore a comparison with the region from the sonic circle to the corner of the wedge was not possible. In figure 13 the wall-density distribution of the present work shows good general agreement with Ben-Dor & Glass. Although the present results show a somewhat lower drop in density behind the sonic circle, the difference is not excessive considering the difficulties in drawing the isopycnics using the finite-fringe method.

Case 7: $M_s = 3.20$, $\theta_w = 20.0°$, $p_0 = 100$ torr, $T_0 = 297.7$ K, SMR. The density contours obtained in the present study (figures 14*a*, *b*) differ to some extent from those reported by Ben-Dor & Glass for a slightly lower M_s, as can be seen from figure 14(*c*). The isopycnics do not converge at the reflected shock in the manner described by Ben-Dor & Glass, nor are any to be seen in state (3). The numerical isopycnics of Kuhl

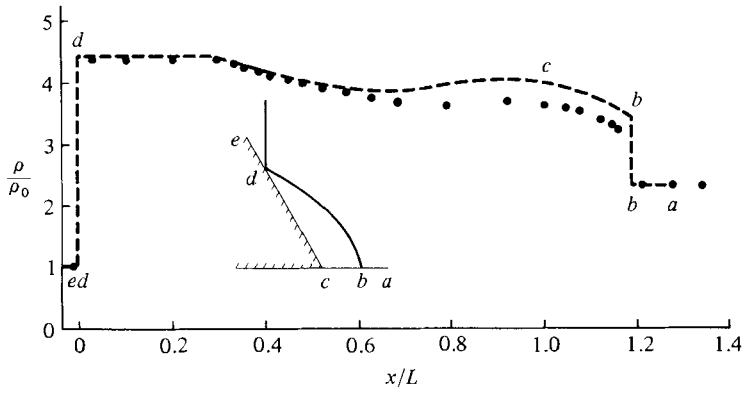

FIGURE 13. Wall-density distribution for the case of regular reflection in argon (case 6): ——, by Ben-Dor & Glass (1980); ●, present experimental results, $\Delta\rho = \pm 2.0 \times 10^{-6}$ g/cm^3, $\lambda = 3472$ Å.

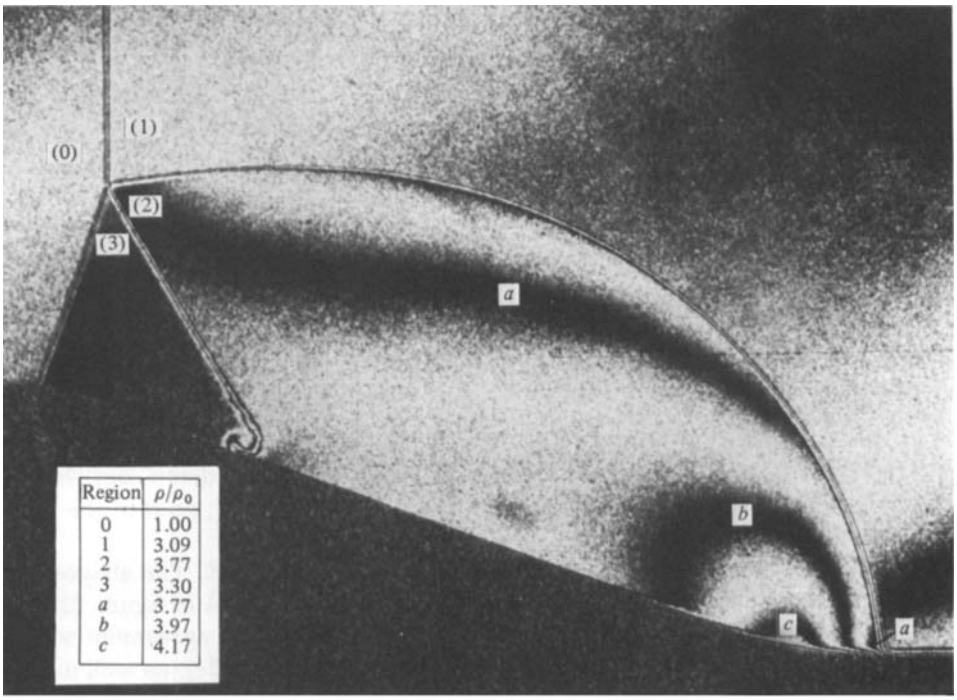

(a)

FIGURE 14. For caption see p. 50.

(1981 private communication) (figure 14*d*) are of the same general shape as those of the present work. Some numerical noise can also be seen. The slipstream is well represented over most of its length, but lacks the beautiful structure shown in the actual interferograms (figure 14*a*,*b*). The few results of Fry *et al.* (1981) (figure 14*e*) do not show the entire flow field or many contours, but agreement is seen with the present work, especially in modelling the slipstream. The values of density are somewhat higher for the present case because of the slightly higher shock Mach number used in the experiments than in the simulations.

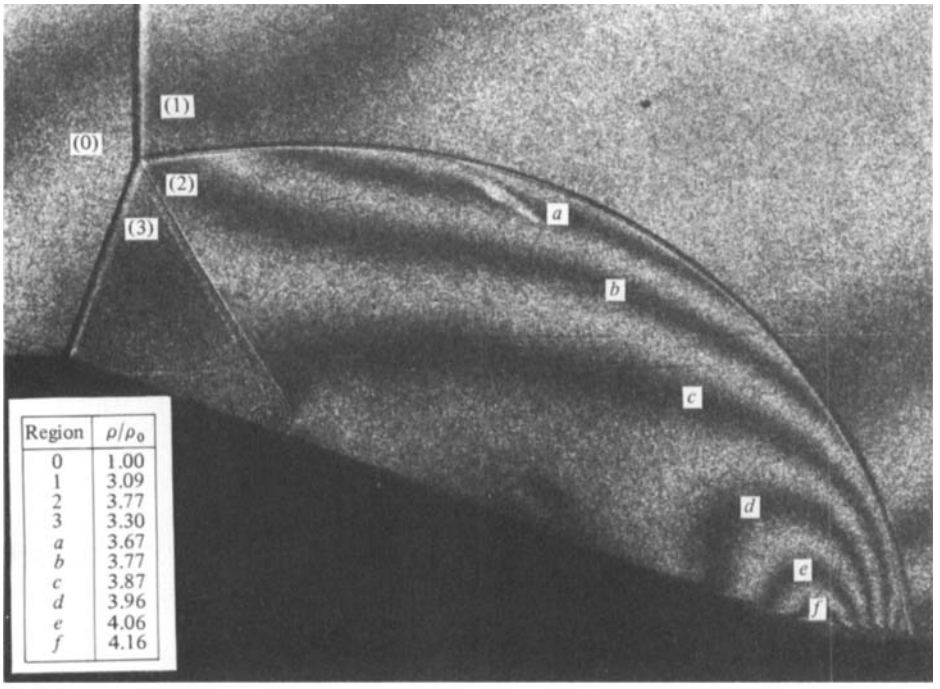

(*b*)

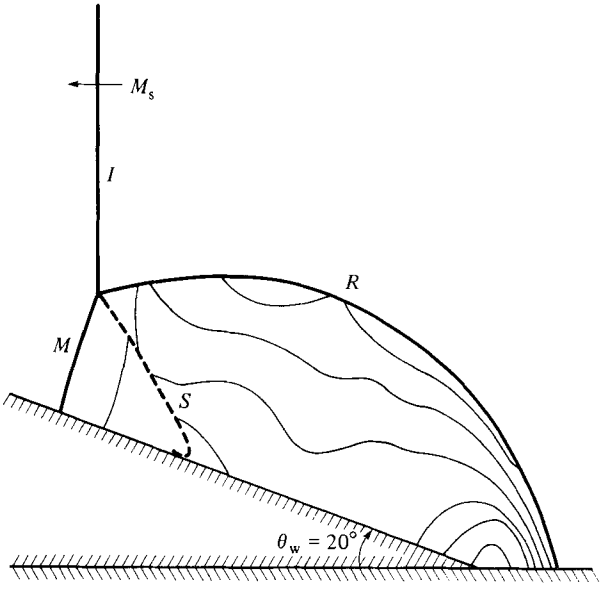

(*c*)

FIGURE 14. For caption see p. 50.

The wall-density distribution in the present study (figure 15) in general agrees well with the results of Ben-Dor & Glass. However, it is clear from figure 14*b* that the slipstream thickness increases with distance from the triple point. Its growth is laminar at first, and then changes to turbulent near the wall. Consequently, although the density in state (2) is greater than in state (3), the transition across the slipstream will be gradual rather than sudden, as shown by Ben-Dor & Glass.

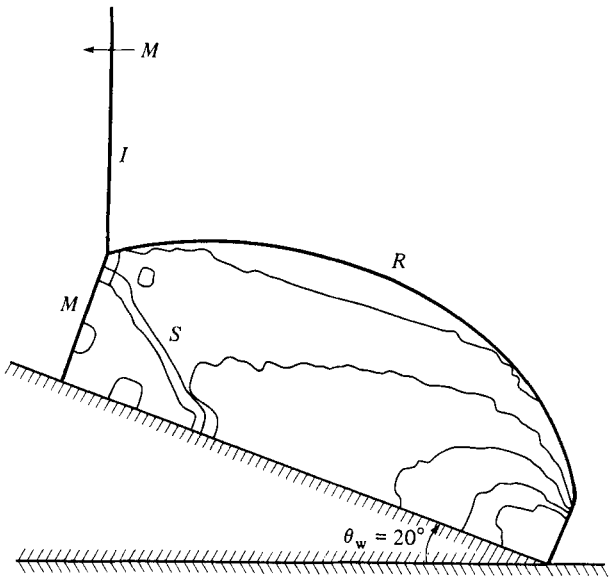

FIGURE 14. Isopycnics for single-Mach reflection in argon (case 7): (*a*) present experimental results, $M_s = 3.2$, $\theta_w = 20°$, $p_0 = 100$ torr, $\rho_0 = 2.15 \times 10^{-4}$ g/cm^3, $T_0 = 297.7$ K, $\lambda = 6943$ Å; (*b*) present experimental results, initial conditions as above, $\lambda = 3472$ Å; (*c*) isopycnics obtained from fringe-shift analysis by Ben-Dor & Glass (1980), $M_s = 2.82$, $\theta_w = 20°$; (*d*) numerical simulation of the density field by Kuhl (1981 private communication); (*e*) numerical simulations of the density contours, by Fry *et al.* (1981).

Case 8: $M_s = 5.07, \theta_w = 30.0°, p_0 = 30.0$ torr, $T_0 = 298.1$ K, CMR. Again differences in the structure of the isopycnics between the present work (figures 16*a*, *b*) and Ben-Dor & Glass (figure 16*c*) can be seen. There is no convergence of the density contours at the kink, as they show. Some agreement can be seen between the results of Fry *et al.* (1981) (figure 16*d*) and the present study, even though there is considerable numerical noise and not all of the flow field is considered. When comparing the wall-density distribution of the present work with Ben-Dor & Glass (figure 17), differences can be seen in the overall shape of the contour, especially at the bow shock, where the drop in density back to state (1) is more gradual than the artificially sharp drop shown by Ben-Dor & Glass.

Case 9: $M_s = 7.10$, $\theta_w = 49.0°$, $p_0 = 15$ torr, $T_0 = 296.3$ K, DMR. For this case it was not possible to increase the initial pressure, because of the limitations of the cold-gas method in producing shock waves. Combustion runs could not be used, since the test-section windows would have been severely burned at such a steep wedge angle. Again owing to the poor index of refraction of argon, very few fringes are observed in the present work (figure 18*a*). In general, however, the structure of the

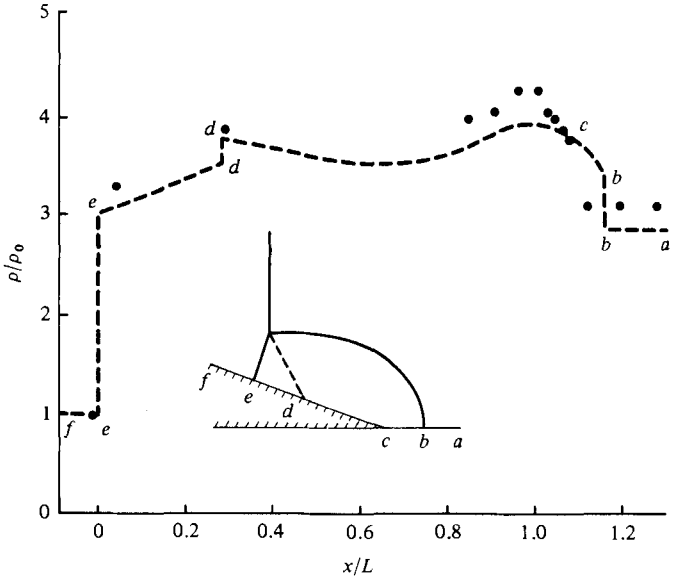

FIGURE 15. Wall-density distribution for the case of single-Mach reflection in argon (case 7): – – – –, by Ben-Dor & Glass (1980); ●, present experimental results, $\Delta\rho = \pm 2.2 \times 10^{-6}$ g/cm^3, $\lambda = 3472$ Å.

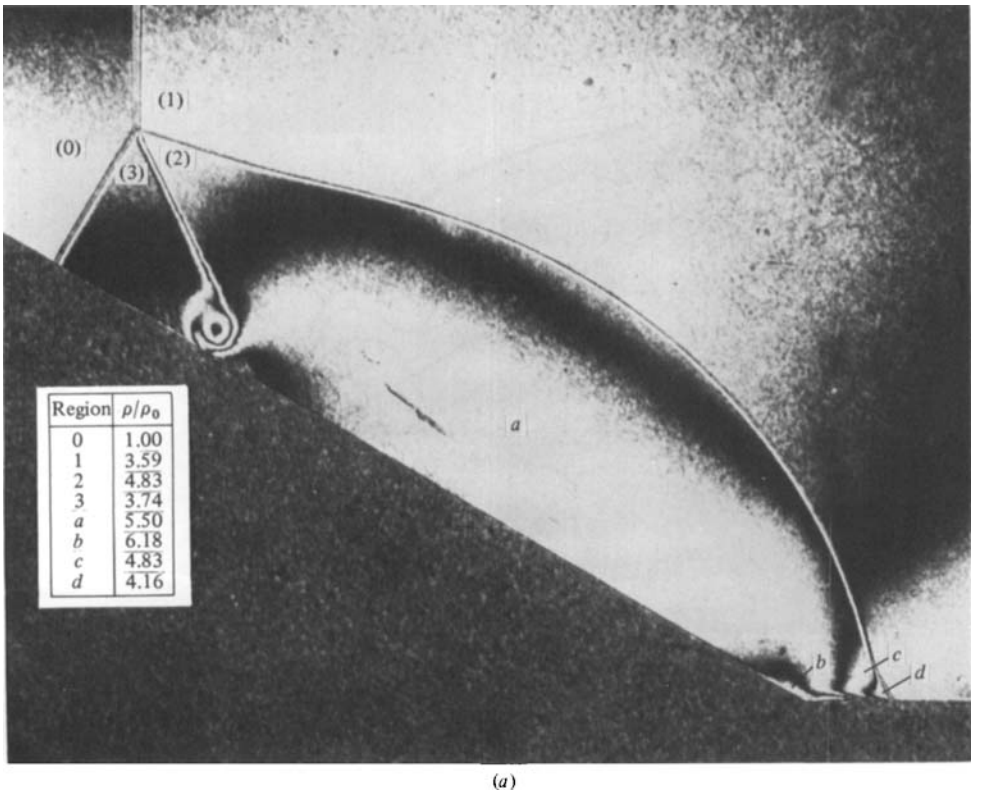

(*a*)

FIGURE 16. For caption see p. 52.

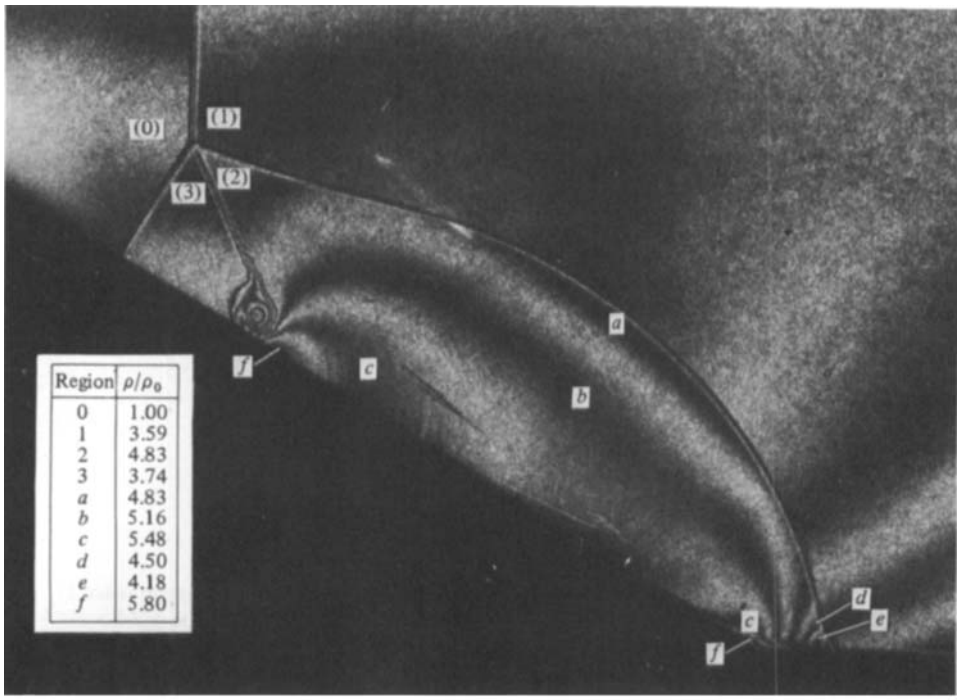

(b)

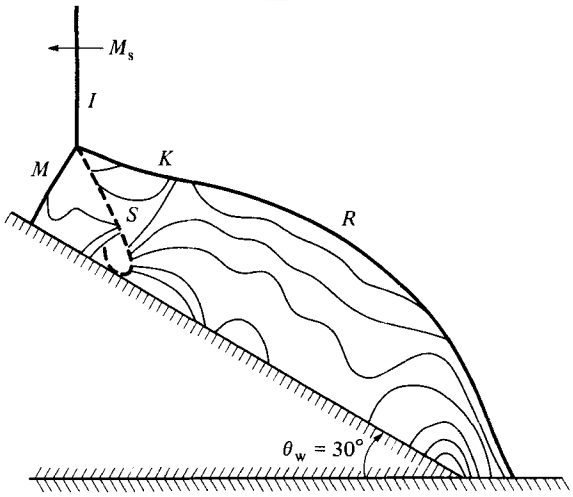

(c)

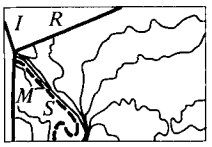

(d)

FIGURE 16. Isopycnics for complex-Mach reflection in argon (case 8): (*a*) present experimental results, $M_s = 5.07$, $\theta_w = 30°$, $p_0 = 30$ torr, $\rho_0 = 6.45 \times 10^{-5}$ g/cm^3, $T_0 = 298.1$ K, $\lambda = 6943$ Å; (*b*) present experimental results, initial conditions as above, $\lambda = 3472$ Å; (*c*) isopycnics obtained from fringe-shift analysis by Ben-Dor & Glass (1980), $M_s = 5.29$, $\theta_w = 30°$; (*d*) numerical simulation of the density contours by Fry *et al.* (1981).

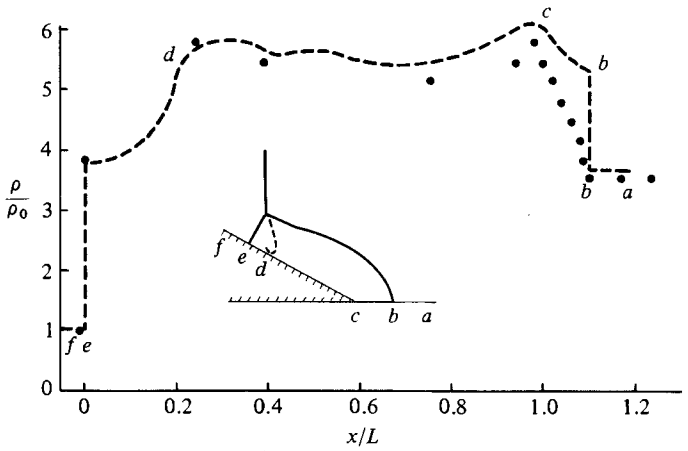

FIGURE 17. Wall-density distribution for the case of complex-Mach reflection in argon (case 8): ------, by Ben-Dor & Glass (1980); ●, present experimental results, $\Delta\rho = \pm 2.0 \times 10^{-6}$ g/cm^3, $\lambda = 3472$ Å.

density contours does not agree with Ben-Dor & Glass (figure 18*b*), especially in the region behind the second Mach stem, where the isopycnic curvatures of Ben-Dor & Glass are the reverse of those in the present study. The numerical simulation (figure 18*c*) by Fry *et al.* (1981) agrees reasonably well with the present work for shock wave and slipstream shapes and positions. The isopycnics are not well represented and suffer from numerical noise.

As for the wall-density distribution (figure 19), there is no significant agreement between Ben-Dor & Glass (1980) and the present study. The major differences are the increase in density behind the second Mach shock, followed by a decreasing density along the wall up to the bow shock.

4. Relaxation effects

One point which was not taken into consideration in our previous experimental work was the fact that the incident shocks have a finite transition thickness. Diatomic gases have various degrees of freedom, which require time to reach equilibrium after being subjected to a shock wave. The translational and rotational degrees of freedom establish an equilibrium distribution of energy in the order of a few collisions, while vibrational relaxation takes up to several hundred collisions to reach equilibrium. In the case of a gas mixture, the vibrational relaxation time of each component may be altered significantly because of the presence of the other. In air the vibrational relaxation time for O_2 may not be influenced by the presence of N_2. However, the vibrational relaxation time of N_2 might be shortened by the presence of O_2. Even more collisions are required to achieve dissociational equilibrium. Vibrational and dissociational relaxation times of air are intertwined in a complicated fashion. An overall relaxation time for the dissociation of air was studied by Schultz-Grunow (1975). In table 2 the calculated vibrational relaxation lengths l_v for pure O_2 and N_2 are given for cases 4 and 5. The overall relaxation length l_d for air is also given. The relaxation lengths were obtained from the interferograms by measuring the distance over which the density in state (1) reached a value of $1-e^{-1}$ (63 %) of the density in state (1′). The relaxation lengths l_v measured in the present study are in fair agreement with the calculated cases for N_2 vibrational relaxation. Therefore the

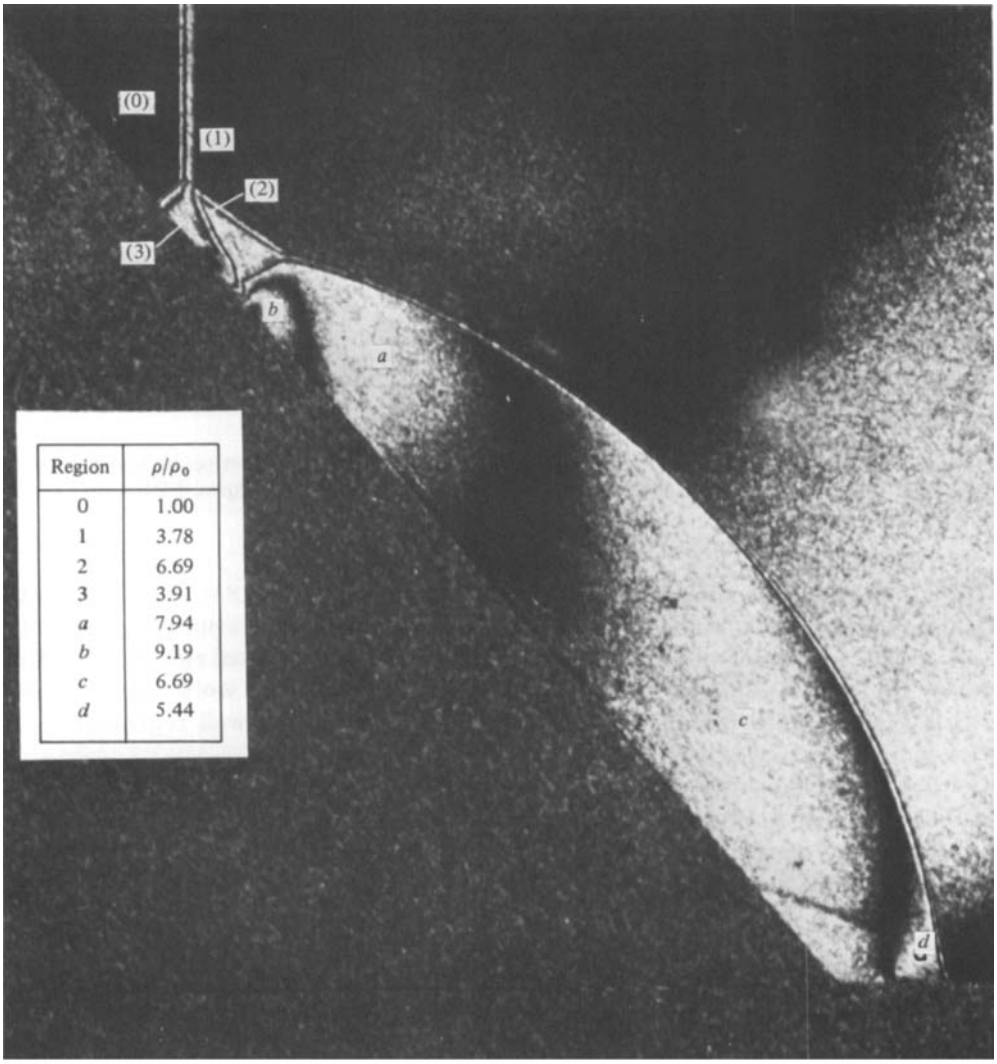

Region	ρ/ρ_0
0	1.00
1	3.78
2	6.69
3	3.91
a	7.94
b	9.19
c	6.69
d	5.44

(*a*)

FIGURE 18. For caption see facing page.

dominant process governing cases 4 and 5 is the vibrational relaxation of N_2. Because the concentration of O_2 in air is only 21 %, its relaxation process would be difficult to observe. For a general discussion of relaxation effects see Shirouzu & Glass (1982).

In cases 4 and 5 the length of the relaxation zone behind the incident shock is considerable when compared to the frozen shock front at the reflection point from the wedge. For these cases a frozen (perfect) gas analysis was used, with $\gamma = 1.40$, to determine the thermodynamic states of the reflection. These basic values and the fringe shifts provided the new densities along the isopycnics.

The use of an analysis based on frozen (perfect) gases is justified in cases 1, 2 and 3, since the Mach numbers were sufficiently low for vibrational relaxation times to be long. In the previous N_2 experiments studied by Ben-Dor & Glass (1979) the vibrational relaxation times were so long that the vibrational modes could be considered as frozen with $\gamma = 1.40$ as a good choice for analysing the flow. Further

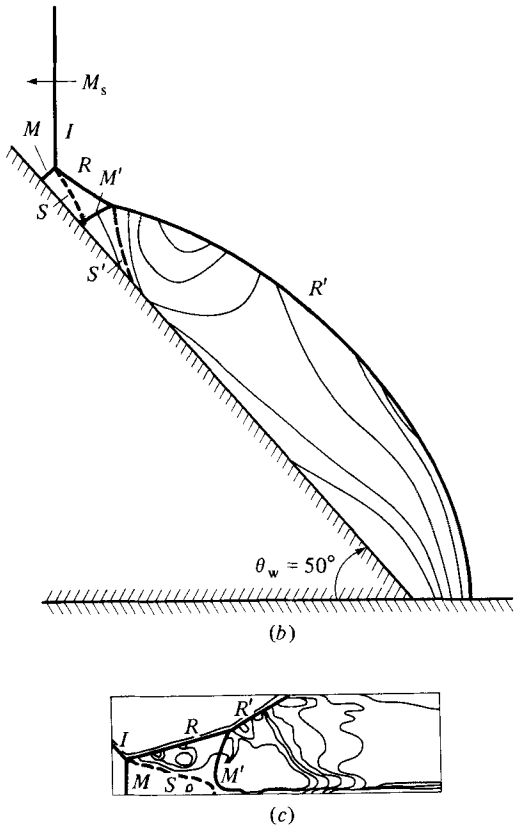

FIGURE 18. Isopycnics for double-Mach reflection in argon (case 9): (*a*) present experimental results, $M_s = 7.1$, $\theta_w = 49°$, $p_0 = 15$ torr, $\rho_0 = 3.29 \times 10^{-5}$ g/cm^3, $T_0 = 296.3$ K, $\lambda = 6943$ Å; (*b*) isopycnics obtained from fringe-shift analysis by Ben-Dor & Glass (1980), $M_s = 7.03$, $\theta_w = 50°$; (*c*) numerical simulation of the density field by Fry *et al.* (1981).

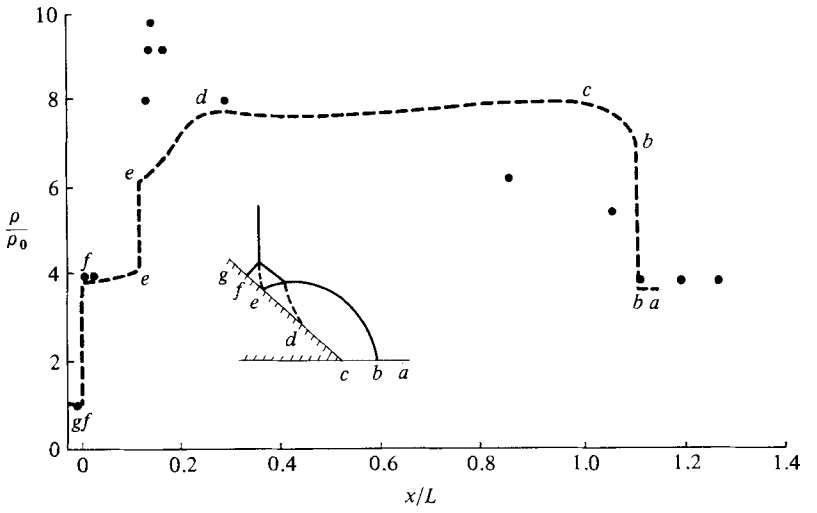

FIGURE 19. Wall-density distribution for the case of double-Mach reflection in argon (case 9); ——, by Ben-Dor & Glass (1980); ●, present experimental results, $\Delta\rho = \pm 4.0 \times 10^{-6}$ g/cm^3, $\lambda = 6943$ Å.

Case	M_s	p_0 (torr)	$l_v(O_2)$ (mm)	$l_v(N_2)$ (mm)	l_d(air) (mm)	l_v(exp) (mm)
4	7.19	60.0	0.10	2.5	33.3	3.7
5	8.70	30.8	0.15	2.9	9.8	3.3

TABLE 2. Comparison of theoretical and experimental, vibrational and dissociational relaxation lengths in air for cases 4 and 5

details on relaxation lengths and other data concerning cases 1, ..., 9 can be found in Deschambault (1983).

5. Conclusions

By using infinite-fringe interferometry it was possible to obtain reliable and basic data for the four different types of pseudostationary oblique shock-wave reflections in air and argon. The results for air are new and have not appeared elsewhere. These have been compared with similar previous work in N_2 (Ando 1981), and the agreement is very satisfactory, as expected. Real-gas effects in oxygen take place at lower shock Mach numbers than in nitrogen, for the same initial conditions, owing to lower characteristic temperatures for vibration and dissociation. Evidence of relaxation processes can be seen for CMR and DMR (figures 8 and 9) at higher shock Mach numbers.

The great advantage of using the infinite-fringe interferogram is that isopycnics are obtained at once, without resorting to polynomial fits of discrete points required in the finite-fringe method. Furthermore, the direct isopycnics provide a much more accurate density distribution along the wedge surface for the same reason.

The new data for oblique shock-wave reflections in argon are much improved compared with our previous results. Here again, the use of a frozen (perfect) gas concept with $\gamma = 1.667$, is, in the range of our experiments, even more valid for shock Mach numbers $M_s \leqslant 7$.

Large sums are spent yearly on computational methods by many countries in order to evaluate the damage caused by spherical shock-wave reflections from chemical explosives. In view of the fact that the agreement between our previous interferometric data and numerical simulations by a number of very able computational-fluid-dynamicists on the simpler problem of wedge flows still leaves a lot to be desired, the spherical-flow computations must be considered with a great deal of caution. Consequently, it is recommended that our new wedge-flow data in air and argon be used to check the improvements in computational programs for frozen and possible non-equilibrium simulations. Agreement would lend a great deal of confidence in the spherical-flow calculations where experimental data may be nonexistent.

We wish to thank Drs A. Kuhl, G. Ullrich, H. Glaz and P. Colella, and G. Ben-Dor for their cooperation and fruitful conversations during the course of the present work. The financial assistance received from the Natural Sciences and Engineering Research Council of Canada, the U.S. Air Force under grant AF-AFOSR 82-0096 and the U.S. Army Research Office is gratefully acknowledged.

REFERENCES

ANDO, S. 1981 *UTIAS Tech. Note* no. 231.

ANDO, S. & GLASS, I. I. 1981 In *Proc. 7th Intl Symp. on Military Aspects of Blast Simulation*, vol. I, pp. 3.6-1–3.6-24.

BEN-DOR, G. & GLASS, I. I. 1978 *AIAA J.* **16**, 1146–1153.

BEN-DOR, G. & GLASS, I. I. 1979 *J. Fluid Mech.* **92**, 459–496.

BEN-DOR, G. & GLASS, I. I. 1980 *J. Fluid Mech.* **96**, 735–756.

BEN-DOR, G., WHITTEN, B. T. & GLASS, I. I. 1979 *Int. J. Heat Fluid Flow* **1**, 77–91.

BLEAKNEY, W. & TAUB, A. H. 1949 *Rev. Mod. Phys.* **21**, 584–605.

BOOEN, W. B. & NEEDHAM, C. E. 1981 *AFWL Tech. Note* NTE-TN-81-001.

BOOK, D., BORIS, J., KUHL, A., ORAN, E., PICONE, M. & ZALENSAK, S. 1981 In *Proc. 7th Intl Conf. on Numerical Methods in Fluid Dynamics* (ed. W. C. Reynolds & R. W. MacCormack). Lecture Notes in Physics, vol. 141, pp. 84–90. Springer.

CHAMPREY, J. M., CHAUSSEE, D. S. & KUTLER, P. 1982 AIAA Paper 82-0227.

COLELLA, P. & GLAZ, H. M. 1982 In *Proc. 8th Intl Conf. on Numerical Methods in Fluid Dynamics* (ed. E. Krause). Lecture Notes in Physics, vol. 170, pp. 175–182. Springer.

DESCHAMBAULT, R. L. 1983 *UTIAS Rep.* no. 270.

FRY, M., TITSWORTH, J., KUHL, A., BOOK, D., BORIS, J. & PICONE, M. 1981 In *Proc. 13th Intl Symp. on Shock Tubes and Waves* (ed. C. E. Treanor & J. G. Hall), pp. 376–384. State University of New York Press.

KUTLER, P. & SHANKAR, V. S. 1977 *AIAA J.* **5**, 197–202.

LEE, J. H. & GLASS, I. I. 1982 *UTIAS Rep.* no. 262.

MACH, E. & SALCHER, P. 1887 *Akad. Wiss. Wien* abt. II, 764–780.

SCHNEYER, G. P. 1975 *Phys. Fluids* **18**, 1119–1124.

SCHULTZ-GRUNOW, F. 1975 *Z. Flugwiss.* **23**, 51–57.

SHIROUZU, M. & GLASS, I. I. 1982 *UTIAS Rep.* no. 264.